Subseasonal Atmospheric Variability and El Niño Waveguide Warming: Observed Effects of the Madden–Julian Oscillation and Westerly Wind Events*

ANDREW M. CHIODI AND D. E. HARRISON

Joint Institute for the Study of the Atmosphere and Ocean, University of Washington, and NOAA/Pacific Marine Environmental Laboratory, Seattle, Washington

GABRIEL A. VECCHI

Geophysical Fluid Dynamics Laboratory, Princeton University, Princeton, New Jersey

(Manuscript received 6 September 2013, in final form 10 January 2014)

ABSTRACT

Westerly wind events (WWEs) have previously been shown to initiate equatorial Pacific waveguide warming. The relationship between WWEs and Madden–Julian oscillation (MJO) activity, as well as the role of MJO events in initiating waveguide warming, is reconsidered here over the 1986–2010 period. WWEs are identified in observations of near-surface zonal winds using an objective scheme. MJO events are defined using a widely used index, and 64 are identified that occur when the El Niño–Southern Oscillation (ENSO) is in its neutral state. Of these MJO events, 43 have one or more embedded WWEs and 21 do not. The evolution of sea surface temperature anomaly over the equatorial Pacific waveguide following the westerly surface wind phase of the MJO over the western equatorial Pacific is examined. Waveguide warming is found for the MJO with WWE events in similar magnitudes as following the WWEs not embedded in an MJO. There is very little statistically significant waveguide warming following MJO events that do not contain an embedded WWE. The observed SST anomaly changes are well reproduced in an ocean general circulation model forced with the respective composite wind stress anomalies. Further, it is found that the occurrence of an MJO event does not significantly affect the likelihood that a WWE will occur. These results extend and confirm the earlier results of Vecchi with a near doubling of the period of study. It is suggested that understanding the sources and predictability of tropical Pacific westerly wind events remains essential to improving predictions of the onset of El Niño events.

1. Introduction

Westerly wind events (WWEs) are zonal wind anomaly events in the western and central equatorial Pacific (Luther et al. 1983; Harrison and Giese 1991; Hartten 1996; Harrison and Vecchi 1997) with typical time (*e*-folding), zonal-spatial, and zonal-wind anomaly scales of 6 days, 1400–2500 km, and 6–7 $m\,s^{-1}$ (up to 15 $m\,s^{-1}$ peak), respectively (Harrison and Vecchi 1997) that have been observed to occur during a wide range of atmospheric phenomena, including tropical cyclones (both single and paired), cold surges from the cold hemisphere, and convective activity associated with the Madden–Julian oscillation (MJO) (e.g., Keen 1982; Harrison 1984; Love 1985a,b; Hartten 1996; Chen et al. 1996; Lin and Johnson 1996). WWEs with substantial wind anomalies in the western and central Pacific waveguide region (within a few degrees of the equator) have previously been shown to precede substantial (up to 1°C) equatorial Pacific cold tongue warming (Vecchi and Harrison 2000; Harrison and Chiodi 2009) when El Niño–Southern Oscillation (ENSO) is in a neutral condition, and to maintain warm central and eastern Pacific sea surface temperature anomalies (SSTAs) in warm-ENSO conditions (Vecchi and Harrison 2000). Other changes along the central and eastern equatorial Pacific seen following western equatorial Pacific WWEs include a deepening of the thermocline and easterly current

*National Oceanic and Atmospheric Administration/Pacific Marine Environmental Laboratory Contribution Number 3825.

Corresponding author address: Andrew Chiodi, NOAA/PMEL, Box 354925, 7600 Sand Point Way NE, Seattle, WA 98115.
E-mail: andy.chiodi@noaa.gov

DOI: 10.1175/JCLI-D-13-00547.1

anomalies in the upper ocean as well as at the surface, consistent with the excitation of intraseasonal downwelling Kelvin waves by the WWEs (McPhaden 2004; Kessler and McPhaden 1995). WWEs are rare in cool-ENSO conditions, in which case their effects are difficult to determine reliably (Vecchi and Harrison 2000).

Composite single WWE wind anomalies applied to ocean general circulation models (OGCMs) have been found to produce cold tongue warming on the order of 0.5°C (Giese and Harrison 1990, 1991; Vecchi 2000; Lengaigne et al. 2002; Harrison and Chiodi 2009). There is general agreement that WWE-induced upper ocean advection anomalies are the primary cause of WWE-driven cold tongue warming. Zonal advection of the background zonal SST gradient has typically been found to be play a dominant role (Schopf and Harrison 1983; Harrison and Schopf 1984; Kindle and Phoebus 1995; Giese and Harrison 1991), although some studies have also found different types of oceanic advection anomalies, including those associated with tropical instability wave modulation of meridional advection (Giese and Harrison 1991) and subsurface advection anomalies (Richardson et al. 1999; Belamari et al. 2003) to be of central importance.

The full role of WWEs in waveguide SST changes has been found to involve coupled ocean–atmosphere dynamical processes, with WWE-driven equatorial Pacific waveguide warming acting to enhance the probability of WWEs (Perigaud and Cassou 2000; Lengaigne et al. 2003, 2004; Vecchi et al. 2006; Gebbie et al. 2007). Thus, the influence of WWEs on ENSO is enhanced by their dependence on the state of the tropical Pacific: WWEs are not best thought of as additive noise to the state of the tropical Pacific (e.g., Lengaigne et al. 2004; Vecchi et al. 2006; Eisenman et al. 2005; Gebbie et al. 2007; Gebbie and Tziperman 2009a,b). Applied with frequency and number consistent with recently observed El Niño years, WWEs have been shown to drive El Niño–like SSTAs (e.g., sustained seasonal ENSO index magnitudes of about 2°C) in realistic ocean circulation models (Harrison and Chiodi 2009).

MJO events are characterized by wind (among other) anomalies that propagate eastward at roughly $5\,m\,s^{-1}$, oscillate in the 30–90-day period range, have zonal scales typical of low-atmospheric wavenumber phenomena, and include significant ($\sim 1.5\,m\,s^{-1}$ average) easterly and westerly surface wind anomalies over the equatorial Pacific waveguide (Madden and Julian 1972). Some have previously hypothesized that MJO events are important to the development of El Niño events because of their possible connection to WWEs (e.g., Slingo et al. 1999; Seiki and Takayabu 2007), while others have taken the view that the surface wind stress variability characteristic of the MJO itself is important to the initiation of El Niño–type tropical Pacific SSTAs. For example, based on OGCM and coupled ocean–atmosphere model results, Kessler and Kleeman (2000) have proposed that MJO-like wind stresses in the western and central equatorial Pacific drive SSTA patterns in the western (cooling of about −0.4°C) and eastern (warming of about +0.1°C) equatorial Pacific that are conducive to the development of an El Niño event. Kessler (2001) found evidence that an extension of MJO-driven surface wind anomalies over the open waters of the western and central equatorial Pacific occurs during El Niño years, which was postulated to enhance the proposed rectification process. Seiki et al. (2009) have also postulated that changes associated with the development of El Niño events cause the MJO-associated surface winds to contribute further to El Niño development. Alternatively, a perspective has developed over the last decade that argues that the MJO contains a "low-frequency tail" (Zavala-Garay et al. 2003) that is correlated with interannual anomalies of MJO variability (Zavala-Garay et al. 2005, 2008) and is important to the development of eastern equatorial Pacific (e.g., the Niño-3 region) SSTA anomalies (Kapur et al. 2012; see also Zhang and Gottschalck 2002). Within this body of literature, it has been claimed that the effects of MJO wind stress anomalies in tropical Pacific SSTA variability dominate those caused by WWEs associated with other intraseasonal atmospheric phenomena because "those wind bursts associated with the MJO are of most importance for interaction with the ocean ENSO, as a large oceanic response is only driven by wind events that are spatially and temporally coherent" (Hendon et al. 2007).

Here we re-examine the relationships among the MJO, WWEs, and equatorial Pacific waveguide warming to gain a better understanding of the role that subseasonal atmospheric processes play in helping to initiate El Niño events. Is the MJO of "most importance" to ENSO, as Hendon et al. (2007) suggest? What is the relationship between the MJO and WWEs? Does the state of the MJO increase the chances that a WWE capable of causing waveguide warming will occur, or does a different kind of relationship exist between WWEs and the MJO? To answer these questions we analyze the historical records of subseasonal wind and SST anomalies in the 1986–2010 period, identifying the times with WWEs and MJO events, and examining the changes in equatorial Pacific SSTA that follow them. The relative numbers of WWEs that occur during and not during MJO events, as well as the numbers of MJO events that do and do not contain a WWE, are also analyzed in the context of a bootstrap Monte Carlo simulation to determine whether there are statistically significant relationships between the timings of these two classes of subseasonal wind events.

Our main focus is on SSTA changes following events that occur in ENSO-neutral conditions [here defined as in Vecchi and Harrison (2000) as |Niño-3| < 0.75°C], since we are interested, inherently and for forecasting purposes, in the processes capable of initiating or at least influencing a transition to the warm-ENSO state. The results of our study are organized as follows. Composites of equatorial Pacific SSTA changes following MJO and WWEs are examined in sections 3 and 4. Results from companion OGCM experiments, in which the model ocean is forced with representative WWE and MJO wind stress anomalies, are compared in sections 5 and 6. Diagnostic analysis of the model results is provided in section 7. Results from a Monte Carlo bootstrap examination of the MJO and WWE co-occurrence statistics are examined in section 8, and a discussion and conclusions are offered in section 9.

2. Data and methods

For information on SST variability, we use NOAA optimum interpolation SST (OISST) version 2 data provided by the National Oceanic and Atmospheric Administration/Office of Oceanic and Atmospheric Research/Earth System Research Laboratory (NOAA/OAR/ESRL) Physical Sciences Division (PSD), Boulder, Colorado, from their website (http://www.esrl.noaa.gov/psd/). OISST data are available on a 1° × 1° grid at weekly resolution. For this study, the data are interpolated to daily resolution to estimate the changes in SSTA that occur over various subseasonal time scales (as described below). SST anomalies are determined using the climatological monthly mean values (base period 1986–2010), linearly interpolated to daily resolution. The same 25-yr base period is used to determine climatological means (and thereby anomalies) throughout this study. We use 10-m wind data from the 12-hourly, 2.5° × 2.5° European Centre for Medium-Range Weather Forecasts (ECMWF) operational forecast dataset (as done in Harrison and Chiodi 2009), which is available online (at http://www.ecmwf.int/products/data; provided at handling costs for research purposes).

The state of the MJO is mainly determined herein using the now commonly referred to real-time multivariate MJO (RMM) index suggested by Wheeler and Hendon (2004, hereafter WH04), which is based on a pair of empirical orthogonal functions of the combined fields of near-equatorially averaged 850-hPa zonal wind, 200-hPa zonal wind, and satellite-based outgoing longwave radiation data. The RMM index is available online at daily resolution (http://www.cawcr.gov.au/staff/mwheeler/maproom/RMM/). By convention, the MJO is considered active when the RMM index amplitude is >1 and inactive when not. We identify "MJO events" from this daily index as those intervals in the 1986–2010 period for which the MJO amplitude is >1 for at least 20 consecutive days. Wind anomaly composites during these "MJO active" times are shown in appendix A (Fig. A1) for each of the eight phases specified by the index, and reveal that statistically significant wind anomalies are seen over the tropical Pacific in each case. We chose to use the 20-consecutive-day requirement since it seemed prudent to focus our consideration on MJO events that reach some basic level of maturity relative to the time scale (~30–90 days) commonly understood to characterize the MJO. Trial showed that this requirement can be omitted without significantly affecting the wind anomaly composite results discussed here. Other results, such as the total number of identified MJO events, are obviously influenced at least somewhat by this requirement, but the conclusions reached regarding the relationship between the MJO, WWEs, and tropical Pacific waveguide warming are not dependent on it. Inspection of the MJO events identified using the RMM index in this manner shows that most of the events do contain most of the eight RMM-type MJO phases, but not every event contains every phase. Before examining the SSTA changes following the RMM-identified MJO events, we also require that the identified MJO events reach their surface westerly phase over the western equatorial Pacific (as discussed in section 3 below).

We found one unusually long (153 days) interval with RMM index amplitude >1 that included three complete sets of phases 1–8. We have counted this interval as three consecutive events. Trial shows that the results are not very sensitive at all to the manner in which this interval is handled. All other RMM-identified events contain no more than one complete set of phases. Notwithstanding this unique event, the duration of the RMM-type MJO events identified range from 20 (an imposed criteria) to 86 days, with an average length of 32 days.

We also report on a second set of results, which, rather than using the WH04 index, instead identify MJO events according to the more traditional Maloney and Hartmann (1998) methods. In this case, a separate MJO index is constructed from the principal components of the first and second empirical orthogonal functions (PC1 and PC2) of 20–80-day band-passed-filtered 850-hPa zonal wind, averaged from 5°S to 5°N around the equator. This index is (with time t in pentads)

$$\text{Index}(t) = \text{PC1}(t) + [\text{PC2}(t+2) + \text{PC2}(t+3)]/2.$$

According to this methodology, MJO events are defined as periods in which >1 standard deviation index peaks are found to be both preceded and followed by index

troughs. The MJO phases (1–9 in this case) are assigned as follows; phase 5 occurs during the index peak, whereas phases 1 and 9 are the preceding and subsequent troughs. Phases 3 and 7 are the increasing and decreasing zero-crossings, respectively, and the even-numbered phases are assigned such that they are evenly spaced between the odd-numbered phases. Thus, by definition in this case, each identified MJO event includes one set of phases numbered 1 through 9, with the latter phases (i.e., 7, 8, and 9) being associated with surface westerlies over the western and central Pacific. Unless noted otherwise, however, the results presented below are calculated using the RMM-based MJO event definition.

The WWE identification and compositing method used here was developed by Harrison and Vecchi (1997) and used previously by Vecchi and Harrison (2000) and Harrison and Chiodi (2009). This method defines WWE events based on three equatorial (5°S–5°N) regions, with boundaries at 130°–155°E, 155°E–180°, and 180°–150°W, for the so-called W-, C-, and E-type WWEs, respectively. WWEs are defined as any interval of 3 or more consecutive days for which the respective WWE region average zonal wind anomaly exceeds $2\,\mathrm{m\,s^{-1}}$. Event composites are based on the identification of a center day (day 0), defined as the event day with the maximum zonal wind anomaly [see Harrison and Chiodi (2009) for more details]. For reference, W-, C-, and E-type WWE composite wind anomalies for all events identified during the 1986–2010 period are shown in appendix A (see Fig. A2).

To examine the effects of the MJO and WWEs on SSTA, we have compiled a dataset consisting of the observed SSTA changes following each type of event in the 1986–2010 period. For WWEs, changes in SSTA are determined relative to the conditions seen 20 days prior to WWE day 0. For consistency, changes following MJOs are determined 20 days prior to the first day that a given MJO event, as defined above using the WH04 index, reaches phase 6 [7 when based on the Maloney and Hartmann (1998) definition], the phase at which surface westerlies begin to dominate the MJO-composite wind anomalies in the tropical Pacific (see Fig. A1). In each case, changes in SSTA at various time lags (e.g., +20, 40, 60, and 80 days) are composited over the events identified to occur in ENSO-neutral conditions. ENSO-neutral conditions are defined herein following Harrison and Chiodi (2009) and Vecchi and Harrison (2000), as the times in which the Niño-3 index (SSTA averaged over the 5°S–5°N, 150°–90°W region) has amplitude less than 0.75°C (i.e., |Niño-3| < 0.75°C). In the case of WWEs, Niño-3 on day 0 is used to determine whether a given WWE event occurs in ENSO-neutral conditions or not. And for the sets of MJO events that all reach their surface-westerly phase over the western Pacific (which provides a basis for the SSTA composites, as described above), the start day of the surface-westerly phase is used to do this. Each of the Maloney and Hartmann-type MJO events reaches its surface-westerly phase over the Pacific (by definition). The vast majority of the RMM-identified MJO events do so as well, but a few do not. When the total RMM-identified group of MJO events is considered, the start day of the MJO events (irrespective of phase) is used. Trial has shown that the results discussed below remain qualitatively similar regardless of which day (e.g., the start of the first MJO phase or, where applicable, the start of the surface-westerly phase) is keyed upon to determine the ENSO state.

The statistical significances of the composite SSTA changes are determined using a Monte Carlo bootstrap procedure, in which random selection (with replacement) from the 1986–2010 record of all possible ENSO-neutral SSTA changes is used to estimate the probability that the magnitude of a given composite SSTA change can be explained by the effects of random selection. The Monte Carlo procedure is explained in more detail in appendix B.

The ocean model used herein is derived from the longstanding NOAA primitive equation OGCM (e.g., Philander and Seigel 1985), and the configuration used here is based on NOAA's Geophysical Fluid Dynamics Laboratory (GFDL) Modular Ocean Model, version 4 (MOM4; Griffies et al. 2003). The global version of MOM4 is the oceanic component of the GFDL Coupled Model, version 2 (CM2; Gnanadesikan et al. 2006), and a tropical Pacific version of the model has been used recently to successfully describe the seasonal cycle of the near surface tropical Pacific by Harrison et al. (2009) and to study the effects of WWE wind stress anomalies by Harrison and Chiodi (2009). To force the experiments described herein, wind data are converted to zonal pseudostress τ^x using the following formula (as done in Harrison and Chiodi 2009):

$$\tau^x = \rho_a C_d |\mathbf{U}| u .$$

Here, air density ρ_a is assigned the value of $1.25\,\mathrm{kg\,m^{-3}}$, the drag coefficient C_d is assumed to have the value of 1.3×10^{-3}, $|\mathbf{U}|$ is the magnitude of the 10-m wind vector, and u is its zonal component.

To examine the effects of MJO wind stress anomalies on tropical Pacific SST, pseudoevent wind stress anomalies are formed from the sequence of MJO-phase composites (phases 1 through 8). Each phase is prescribed to last 5 days, for a total of 40 days of anomaly forcing. Wind stress anomalies are applied to the model beginning with phase 1. The effects of using a different starting point

(e.g., starting with phase 6 and proceeding in modulo order) were examined but are not discussed since they produce results qualitatively similar to those described herein. We have also experimented with prescribing the duration of the phase according to the actual time spent in each in the identified MJO events, but find results qualitatively similar to those produced by the 5-day duration composites are yielded in this case (as described in the results section).

For comparison, the effects of WWE-type wind stress anomalies are also examined with OGCM experiments following the methods of Harrison and Chiodi (2009), in which case the respective daily WWE–wind stress anomaly composites from event days −20 to +20 are applied to the model. In both the MJO and WWE experiments, the model is first spun up to realistic climatological conditions [as described in detail in Harrison et al. (2009)], and the wind stress-driven SSTAs are determined by comparing the model SST fields produced by integrating the model with and without the respective wind stress anomalies.

3. Observed SSTA changes following MJO events

We identified 64 MJO events that occurred in the 1986–2010 period during ENSO-neutral conditions and 61 that reached their westerly surface phase (i.e., phases 6, 7, and 8) during ENSO-neutral conditions. The composite change in SSTA following the 61 MJO events, keyed on the beginning of the westerly surface phase (phase 6), are shown in the left-hand panels of Fig. 1, with shading where the composited SSTA changes are statistically significant ($p > 0.95$) based on Monte Carlo bootstrap methods. The composite SSTA change 20 days after the start of MJO phase 6 (top-left panel) shows little statistically significant anomaly that persists to the following +40-day composite, which, like the +20-day case, shows rather little change from starting conditions in the tropical Pacific. The subsequent +60-day composite shows some warming in the eastern equatorial Pacific between 140° and 100°W with amplitudes of 0.2°–0.4°C, which are not yet statistically significant. This warming pattern intensifies by the +80-day composite, however, becoming statistically significant then.

Of these 61 MJO events, 43 have an embedded WWE and 18 do not. The composite changes in SSTA following MJOs without a WWE are shown in the center panels of Fig. 1. Examination clearly shows that, in an average sense, statistically significant warming does not follow the 18 MJO events that do not contain a WWE.

On the other hand, the SSTA changes that follow MJO events containing at least one W-, C-, or E-type WWE (Fig. 1, right) produce some isolated regions of warming in the central equatorial Pacific in the +20-day composite, which can be seen to broaden to an elongated pattern of >0.2°C warming located between the date line and 110°W in the +40- and +60-day composites, and continues to intensify as it moves eastward during the next weeks, resulting in substantial (0.4°–0.6°C) and statistically significant warming in the eastern equatorial Pacific by the +80-day composite.

We also used the methods of Maloney and Hartmann (1998; MH98 hereafter) to identify 68 MJO events that occur in ENSO-neutral conditions during the study period. The corresponding +80-day composites of SSTA change are shown in Fig. 2 for the 47 MH98-identified MJO events that do and 21 MH98-identified MJO events that do not contain a WWE. The corresponding +80-day RMM-based SSTA-change composites (as discussed above) are also shown in this figure for comparison. Based on the MH98 definition, very little equatorial Pacific warming is seen following the identified MJO events regardless of whether they do or do not contain a WWE.

Inspection showed that most (70%) of the days included in the MH98 set of ENSO-neutral MJO events occur during times with RMM index amplitude >1, and there is generally good agreement on the phase of the MJO during these times. Thus, although the two methods identify many of the same MJO events, the differences are sufficient to make the amounts of warming that follow an MJO event that contains a WWE dependent on the MJO identification method used. More importantly, however, each set of composite results agrees that MJO events that do not contain a WWE are not followed by equatorial Pacific waveguide warming.

4. Observed SSTA change following WWEs

A total of 98 W-type WWEs are identified in the 1986–2010 period during ENSO-neutral conditions. The composite changes in SSTA that follow these WWEs are shown in the left-hand panels of Fig. 3, where it can be seen that a small (<0.2°C), but statistically significant warming occurs in the central equatorial Pacific in the first 20 days following these WWEs that intensifies and moves eastward over the following weeks, resulting in a coherent pattern of equatorially trapped warming in the +80-day composite that spans much of the central and eastern equatorial Pacific and has amplitudes >0.4°C in the eastern equatorial Pacific.

The composite SSTA changes following C- and E-type WWEs that occurred in ENSO-neutral conditions over the same 25-yr period are shown in the center and right-hand panels of Fig. 3, respectively (based on 105 C-type WWEs and 52 E-type WWEs). Some differences and similarities between these and the W-type composite

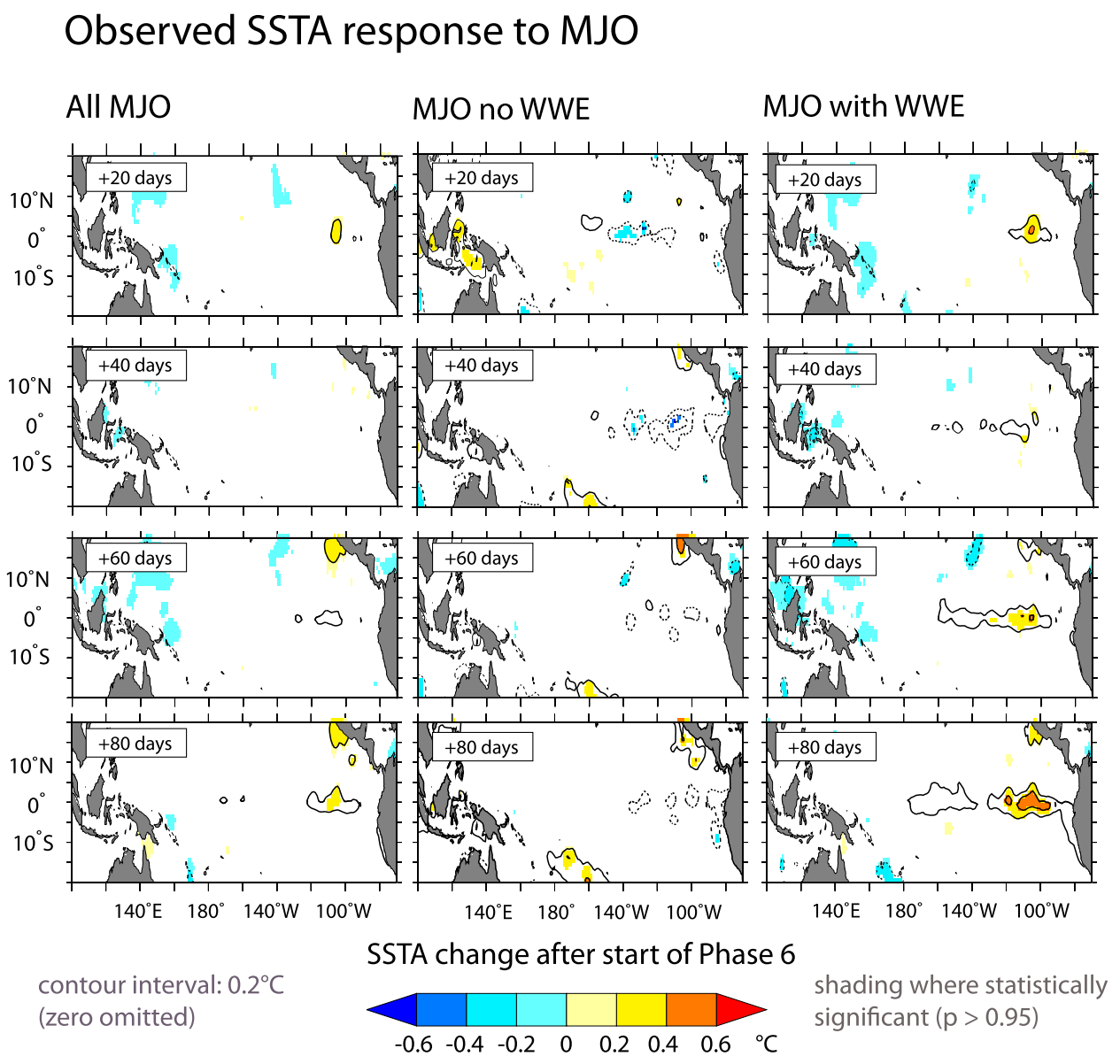

FIG. 1. Composite SSTA change following the MJO events that occurred in ENSO-neutral conditions (|Niño-3| < 0.75°C) from 1986 to 2010. Results shown separately for (left) all 61 ENSO-neutral MJO events, (center) the 18 MJO events that do not contain an embedded WWE, and (right) the 43 that do contain a WWE.

are evident. For example, the warming amplitudes following the C-type (E-type) events are somewhat smaller (larger) than seen in the W-type case, and the coherent cooling seen west of the date line in the W-type composites is not evident to the same degree in the C- and E-type composites. However, the same basic picture emerges from each of these three composite sequences; in an average sense, warming anomalies with amplitudes of a few to several tenths of a degree Celsius appear in the central and eastern equatorial Pacific following each of these three types of WWEs.

For reference, the +80-day changes in Niño-3 that follow each of these types of WWEs are listed in Table 1. Results for all WWEs occurring in ENSO-neutral conditions show that on average, the Niño-3 SSTA index warms by a statistically significant (at the 95% level) few tenths of a degree Celsius following each of these three types of WWEs (first column). Results also show that warming is seen regardless of whether the WWEs occur during MJO events (second column) or not (third column); and although somewhat larger warming amplitudes were seen following the WWEs that occurred

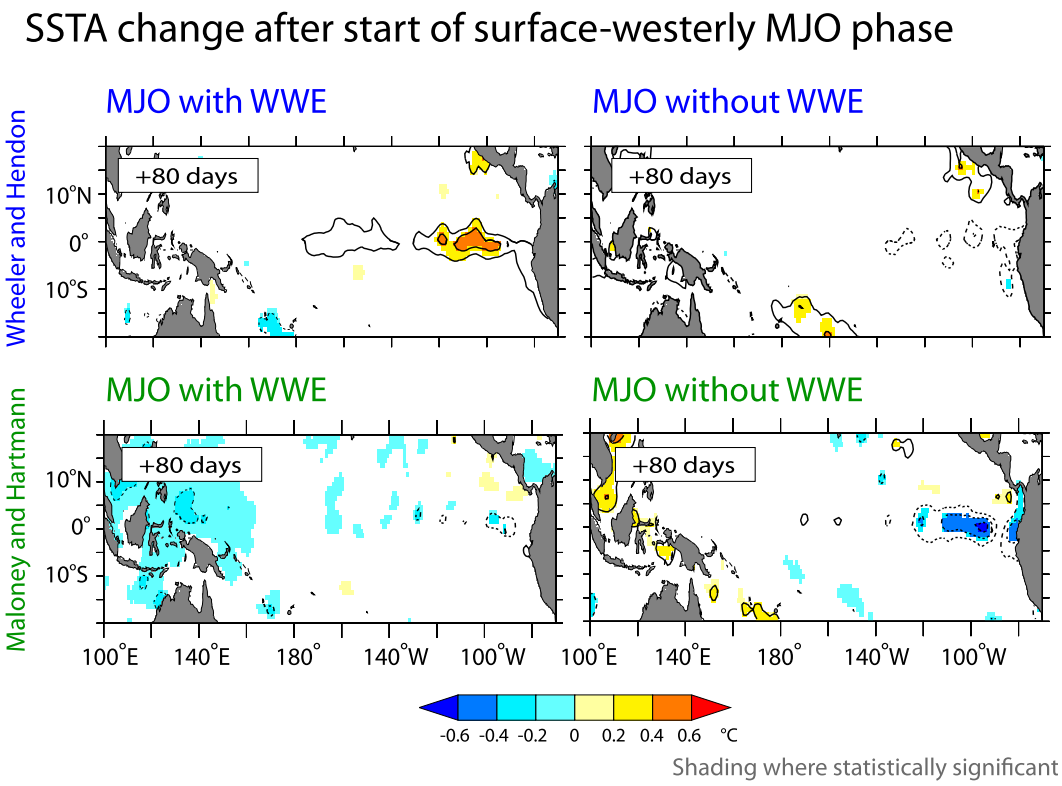

FIG. 2. (top) As in Fig. 1 bottom-right and bottom-center panels (+80 days), but are based on the WH04 MJO index. (bottom) Same as (top), but for the case the MJO events are identified using the MH98 index.

during MJO events, especially in the E-type composite, the differences between these and the composite Niño-3 changes following WWEs that did not occur during an MJO event are not statistically significant at the 90% confidence level. At lower levels (e.g., 80%), the E-type difference, which is based on the fewest number of samples, may become statistically significant, but the differences seen for the W- and C- types remain well within the range expected from the effects of random selection (even at the 66% confidence level).

In the review process, because the range of Niño-3 SSTA defined by us as "neutral" contains conditions that might be considered moderately warm (e.g., 0.5° < Niño-3 < 0.75°C), and the frequency of WWEs has previously been shown to increase with ENSO SSTA (as discussed below), the question of whether or not the warming seen in these composites might be influenced by longer-time-scale processes associated with El Niño onset, such as a slower Gill-type (Gill 1980) response to warm tropical SSTAs, came up. To examine this, we have recomputed the composite SSTA changes following WWEs using, this time, just the portion of identified WWEs that occur in the cold half of the ENSO-neutral regime (i.e., −0.75° < Niño-3 < 0°C). In this case, we find that the numbers of WWEs identified are roughly half of those found in the full-neutral case, indicating that the effects of increasing ENSO SSTA on WWE frequency are not yet strongly felt in the |Niño-3| < 0.75°C regime (e.g., 50 out of 105 C-type events reside in the cold half of this regime). We also find that the composite waveguide warming following WWEs in the cold-neutral case is at least as strong as that seen in the full-neutral case, strongly suggesting that it is the WWEs, rather than effects of processes such as the Gill-type response to warm tropical SSTAs, that drives the warming seen in these composites. The model results described below also support this view.

5. Model response to composite MJO wind anomalies

The effects of MJO wind stress anomalies applied to a realistic ocean general circulation model are examined in the experiments described here. In each experiment, we first formed composite wind stress anomalies for each phase of the MJO based on the daily anomalies seen in the identified MJO events that occurred in ENSO-neutral conditions. Next we form a pseudo-MJO-event composite based on the eight different phase composites by prescribing that each phase lasts for 5 days. The resulting 40-day wind stress anomaly composite (shown in Fig. 4,

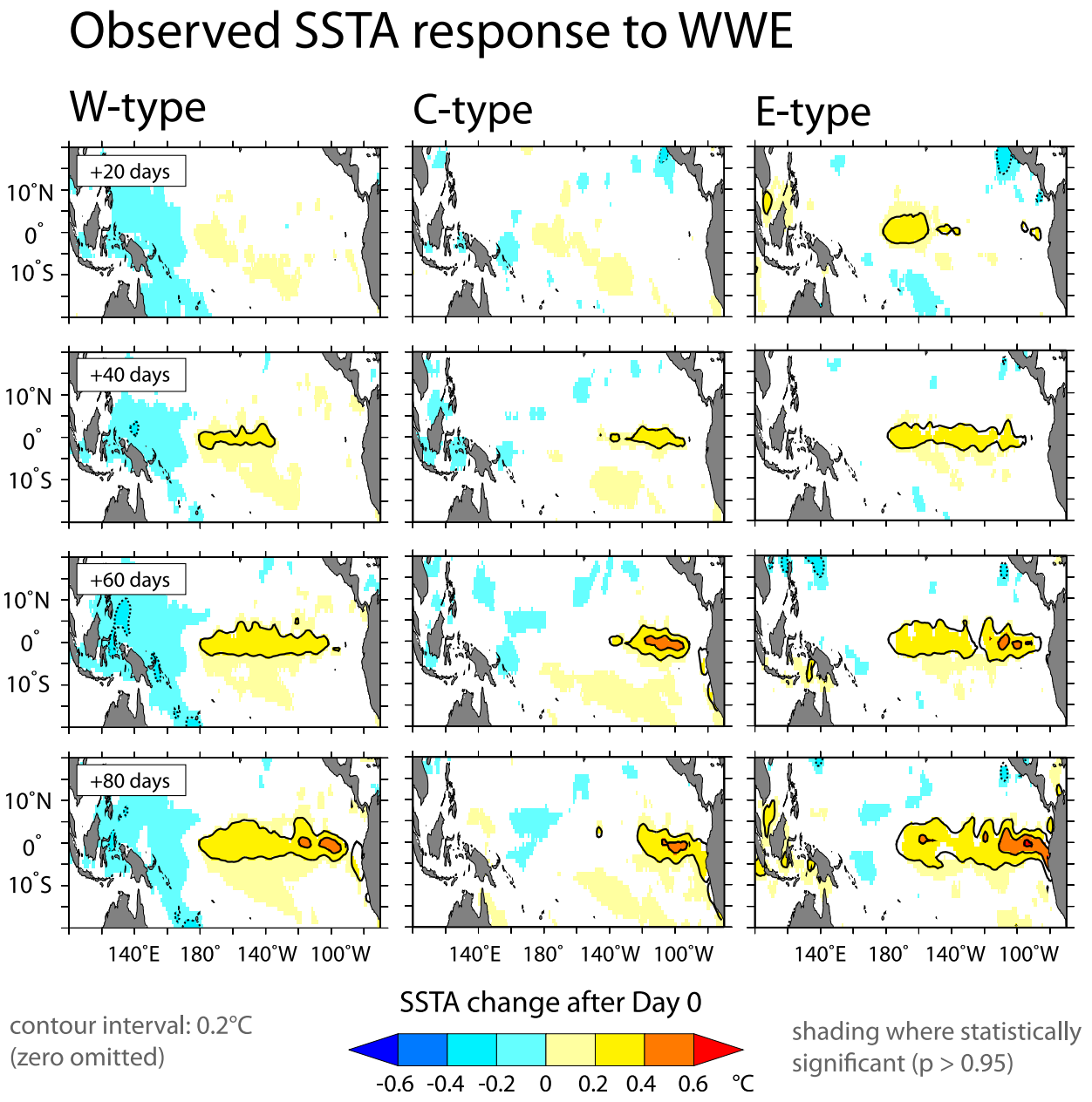

FIG. 3. Composite SSTA changes following (left) W-, (center) C-, and (right) E-type WWEs that occurred in ENSO-neutral (|Niño-3| < 0.75°C) conditions in the 1986–2010 period.

top) is then applied to the model. We have also looked at what happens when the phase duration is specified according to the time spent, on average, in each phase during the identified MJO events, but found that the results are very similar to those produced by the 5-day phase composite (discussed further below).

Preliminary experiments showed that the model results remain qualitatively similar regardless of which season the wind stress composites are applied in. For brevity, we discuss results from a single case (June) in which the wind composites are applied during a season typically associated with the El Niño "onset" stage (Larkin and Harrison 2002). The conclusions reached herein are not affected by the choice of month in which the wind anomalies are applied to the model.

We discuss results from three different experiments that are procedurally similar except that in the first, all 64 ENSO-neutral MJO events that are identified using the RMM index are used to form the pseudoevent composite; in the second, just those MJO events with

TABLE 1. Niño-3 index change (°C) 80 days following a WWE that occurs in regional SSTA conditions.

	All WWEs	MJO active	MJO inactive
W-type	0.24	0.29	0.21
C-type	0.18	0.22	0.16
E-type	0.31	0.41	0.17

embedded W-, C-, or E-type WWEs are used; and in the third, only the MJO events that do not contain a WWE are used.

The evolution of SSTA in the months following the application of the composite based on all of the 64 MJO events that occurred in ENSO-neutral conditions is shown in the left-hand panels of Fig. 5, where it can be seen that only relatively modest amplitude (<0.2°C) changes in SST are driven in the model and last until days +60 or +80 in this case.

The SSTAs driven by the composite based on MJO events that do not contain any WWEs are shown in the center panels of in Fig. 5, and the composites based on MJO events that contain either a W-, C-, or E-type WWEs are shown in the panels on the right-hand side of this figure. Comparison of these results reveals change in character depending on whether the original MJO events did or did not contain a WWE. The MJO wind stress composite with a WWE produces a patch of small-amplitude (0.1°–0.2°C) equatorially trapped warming near the date line that can be seen in the +40-day panel (right-hand panels, second row), which is followed by a somewhat stronger, albeit still relatively modest (0.2°–0.4°C) patch of warming in the cold tongue region (e.g., ~140°–110°W) in the +60- and +80-day panels (right-hand panels, bottom two rows). In contrast, the experiment based on the MJO events that do not contain a WWE (center panels) does not show warming in these regions at these times.

Comparisons with the companion SSTA changes seen following MJO events in the observations show some differences and similarities in each case. In the 64-MJO-event case, the warming seen in the composite of observed SSTA changes (Fig. 1, left) shows somewhat larger amplitude warming at +80 days compared to the model. This could be attributable to the aliasing of other sources of warming (e.g., previous WWEs), errors in the composite wind stress, or model biases. The observed SSTA changes following MJOs with WWEs (Fig. 1, right) show a small patch of warming in the 110°–100°W

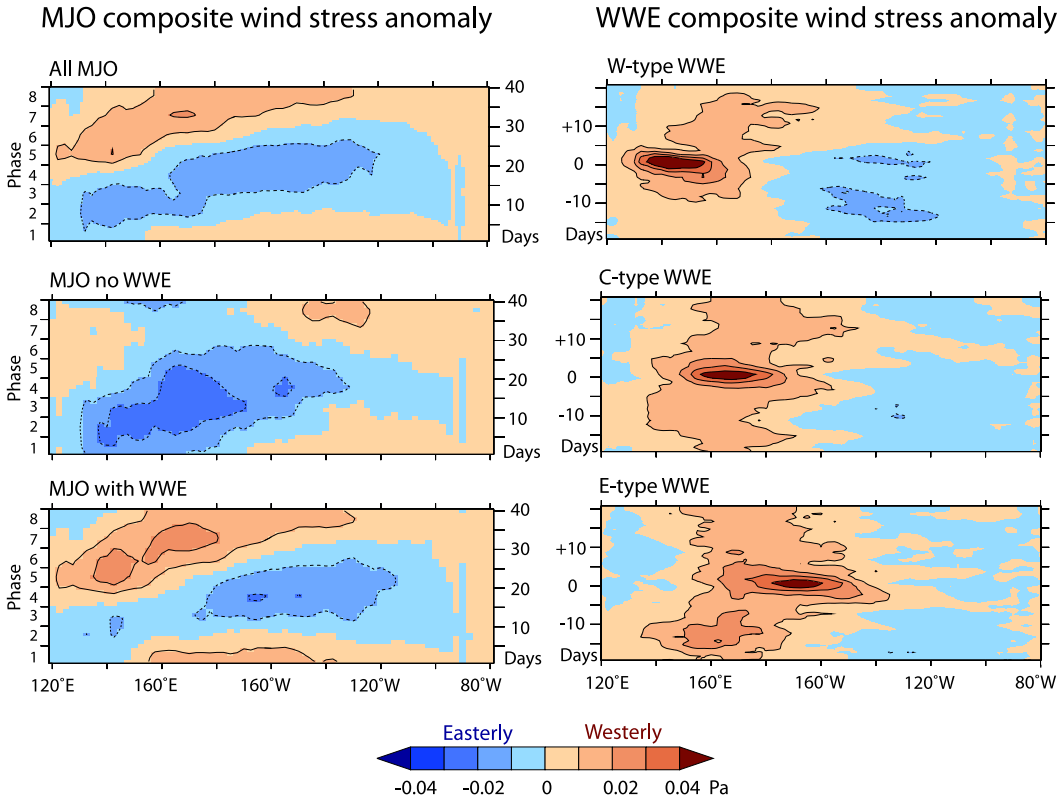

FIG. 4. (left) Composite MJO wind stress anomalies for all MJO events and MJO events without and with WWE. (right) The W-type, C-type, and E-type WWE composite wind stress anomalies. All are averaged over 2°S–2°N.

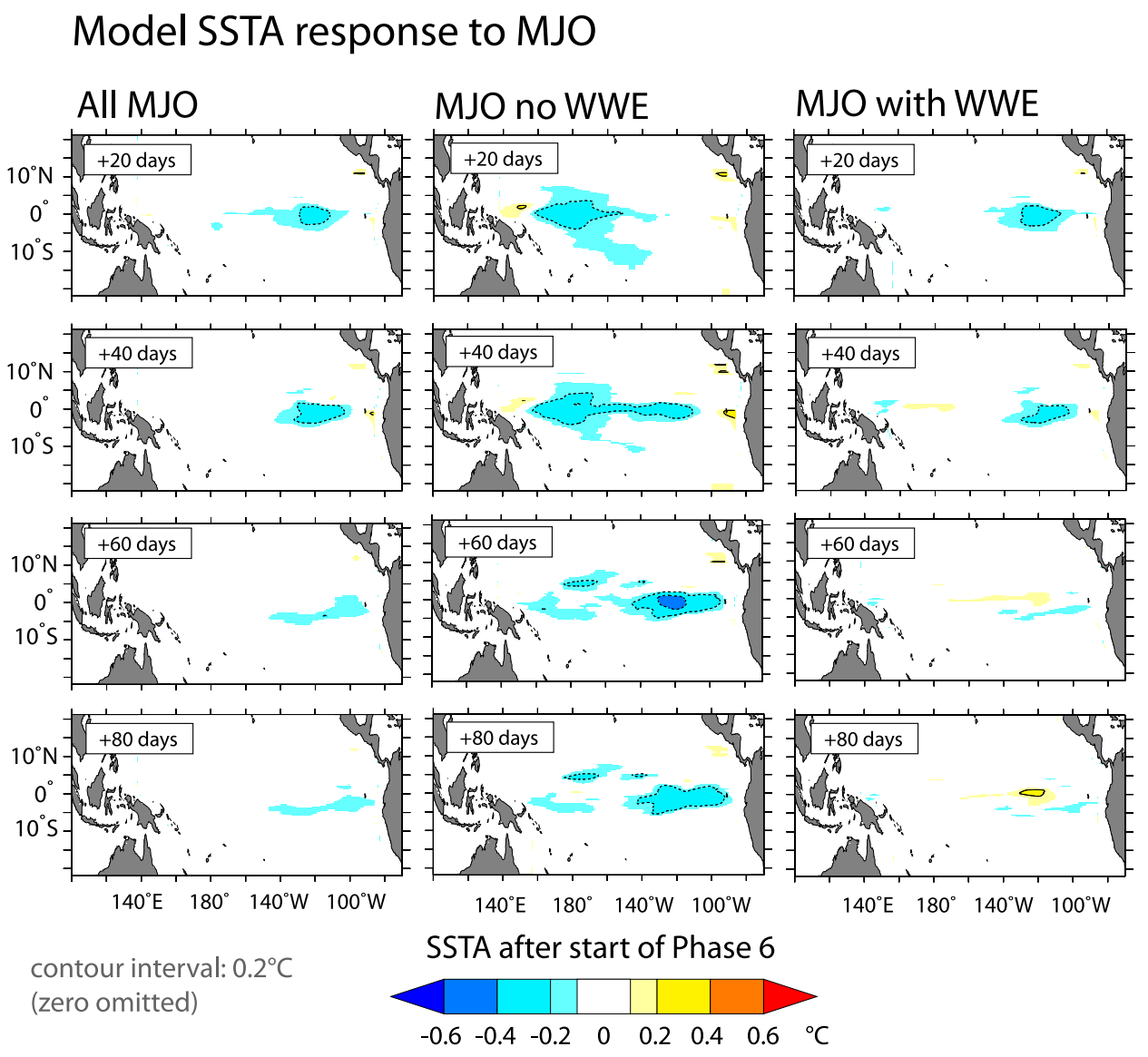

FIG. 5. Change in model SSTA following the application of the composite MJO wind stress anomaly.

region in the +20-day composite that is not reproduced in the model (Fig. 5, right), which could likewise be attributable to, for example, the effect of several prior but closely timed WWEs. Also, the cooling amplitudes seen in the model following a MJO-wind anomaly composite that does not contain a WWE (Fig. 5, center), which peak in the 0.6–0.8°C range, are larger in magnitude (by about 0.2°C) and broader in scale than the cooling seen in the companion +20- and +40-day observation-based SSTA-change composites (Fig. 1, center). Even with these differences, however, the MJO model experiments and composite analysis have in common the fact that, in each case, the SSTA changes that include the effects of WWEs lead to cold tongue warming on the order of a few tenths of a degree following the wind event. The results for MJO events that do not contain a WWE, however, do not show this type of warming.

As mentioned above, we have also repeated the experiments discussed above after modifying the idealized MJO composite so that the number of days spent in phase varies (at 6-h resolution) according to the average time spent in each phase in the identified MJO events. The average duration across all phases turns out to be 4.5 days, ranging from 5.5 days in phase 6 to 3 days in phase 4. Qualitatively similar results are obtained in the varying-duration and equal-duration cases (cf. Fig. C1). The character of SSTA produced in the model depends much more on whether the MJO does or does not contain

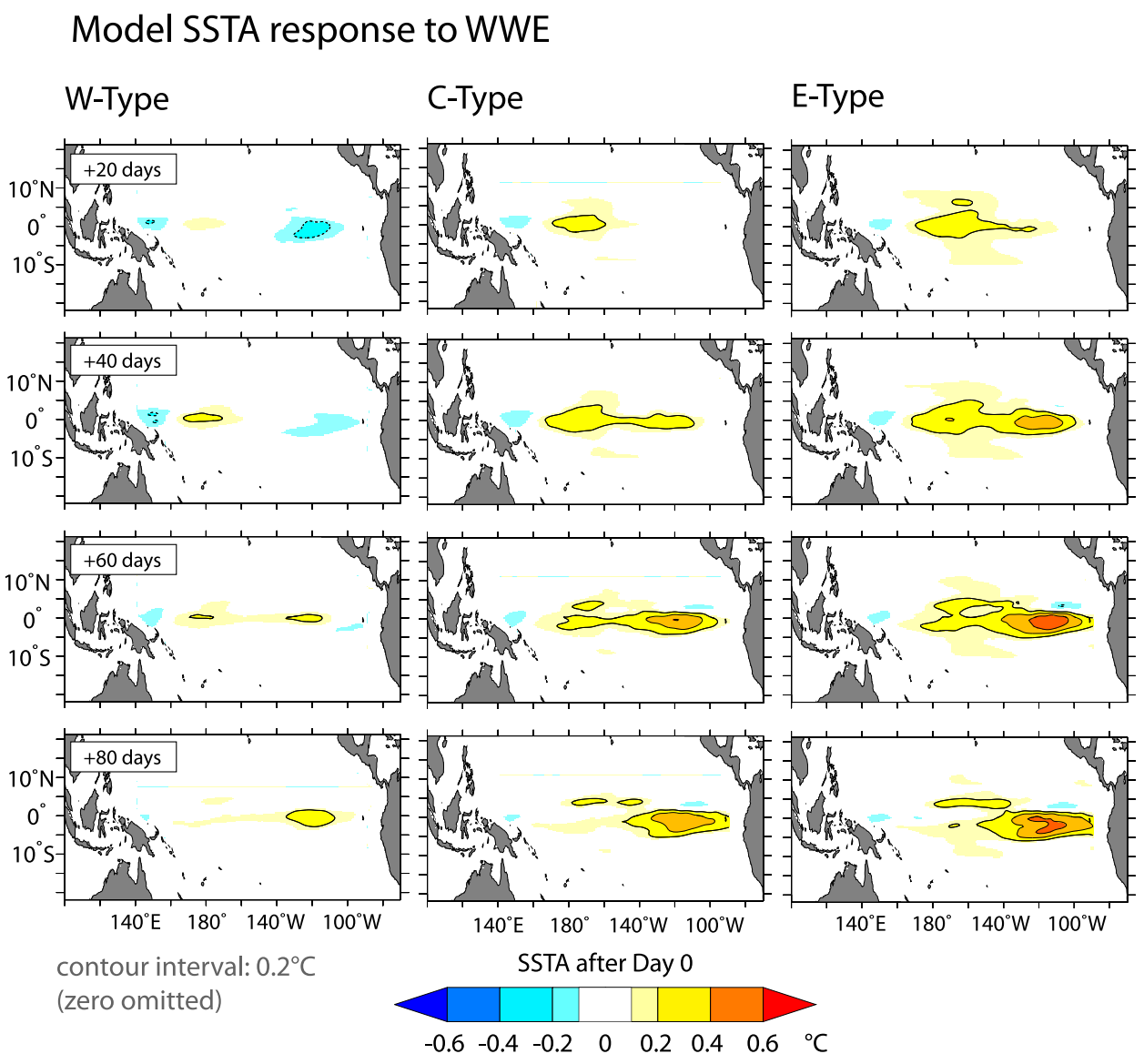

FIG. 6. Model SSTA following the application of a composite WWE wind stress anomaly.

a WWE than it does on these types of details of the observed MJO-phase duration.

6. Model response to WWE wind stress anomaly

The SSTA anomalies driven in the ocean model by composite W-, C- and E-type WWE wind stress anomalies can be seen in Fig. 6. As in the MJO base case, the wind anomalies in these experiments are applied for 40 days. For each WWE type, equatorially trapped warming on the order of a few tenths of a degree Celsius is seen following the WWE in the equatorial central Pacific and later in the equatorial eastern Pacific, at somewhat greater amplitude than seen earlier around the date line. It is notable that this set of composite wind stress anomalies, which is keyed specifically on WWEs rather than the MJO phases, drives warming patterns that are more coherent and larger than, but nonetheless similar in character to, those driven in the model by the "MJO with WWE" wind stress composites. For example, in each case, an initial near-equatorial warming is seen around the date line (i.e., in the +20- or +40-day panels) that is followed (at +60 or +80 days) by stronger warming in the equatorial eastern central Pacific. Some differences are noticeable also. Less initial warming is seen in the MJO with WWE model experiments than is seen in the experiments that key specifically on WWEs, which perhaps is not surprising given that the applied MJO wind anomaly

composite begins in its surface-easterly wind anomaly phase and such easterlies, which should be expected to cool the central and eastern Pacific, are not, in general, a characteristic of WWE wind anomalies.

Comparison of the WWE-based model (Fig. 6) and observational results (Fig. 3) reveals some similarities and differences. But keeping in mind the many possible reasons for discrepancies of about 0.2°C (e.g., wind stress error, model bias, and aliasing SSTA changes caused by other events in the observations), it can be said that the upper ocean circulation changes driven in the model by the composite WWE wind anomalies cause warming of SSTA in the central and eastern equatorial Pacific that is at least roughly consistent in terms of magnitude, timing, and character with the changes observed to follow these types of WWEs in an average sense. This is consistent with results previously discussed by Vecchi and Harrison (2000) and Harrison and Chiodi (2009).

We also looked at the effects of using WWE wind anomalies composited over just those WWEs that occurred and did not occur during an MJO event, but found that very similar SSTAs were driven in each case. This can be seen in Fig. 7, where the equatorial SSTA changes following the application of two C-type WWE composites (embedded in MJO and not) are shown in the time–longitude perspective. We also ran the corresponding W- and E-type experiments, and found that similarly small differences in SSTAs are seen in these cases between the MJO-embedded and not-embedded composites (not shown for brevity). The state of the MJO does not appear to importantly affect the ability of the WWEs to cause warming of the central and eastern equatorial Pacific.

Following up on comments made in the review process, we have also looked at whether the westerly wind stresses seen in the WWE wind stress composites at more than about a week removed from day 0 (see Fig. 6, bottom three panels) should be considered part of the WWEs, or perhaps are instead indicative of the presence of other longer-time-scale atmospheric processes associated with ENSO onset such as the traditionally invoked Gill-type response to warm tropical SSTA. Like in the WWE–SSTA composite case described above, we have recomposited the WWE wind stress anomalies this time just using those events that occur in the cold half of the ENSO-neutral regime and find very similar structures beyond day ±7 (i.e., enhanced westerlies in the WWE definition region) in both the cold-neutral ($-0.75° <$ Niño-3 < 0°C) and full-neutral ($|$Niño-3$| <$ 0.75°C) cases. This suggests that these features are associated with the WWEs themselves. We have also confirmed that similar SSTAs are also produced in the model when forced by these two sets of WWE wind

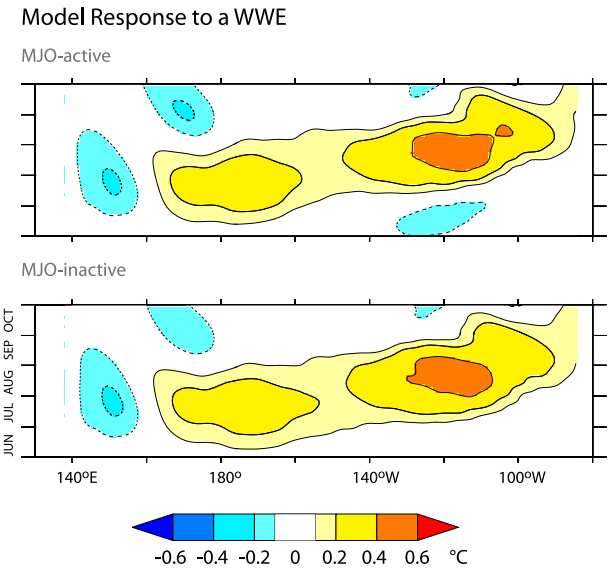

FIG. 7. Model SSTA following application of a C-type WWE wind anomaly. (top) Only WWEs that occurred in ENSO-neutral and MJO-active conditions were used in the composite used to drive the anomaly, and (bottom) as in (top), but for ENSO-neutral and MJO-inactive conditions.

stress anomalies (not shown for brevity). We find in further experiment that reducing the amount of westerly wind stress forcing in these experiments by restricting the number of WWE days applied to, for example, ±5 or ±10 days does reduce, but not eliminate, the amount of warming seen following a single WWE. This serves as a reminder that the length scales used to describe WWEs, both herein and previously (e.g., Harrison and Vecchi 1997; Vecchi and Harrison 2000), are *e*-folding time scales, and thus substantial amounts of variability (37%) should be expected to remain outside of this nominal length scale.

In summary, oceanic waveguide warming is seen in the model following the application of W-, C-, and E-type WWE wind anomaly composites, regardless of whether the WWEs occur during an MJO or not. Waveguide warming with similar character is also seen in the case of an MJO that contains a WWE, but waveguide warming is not seen following the MJO wind anomalies that do not contain a WWE. In these model experiments, WWE wind anomalies are necessary to drive cold tongue warming; MJO wind anomalies are not necessary to drive cold tongue warming.

7. Model diagnostics

In this section we further explore the oceanic processes that allow equatorially centered WWEs to warm the oceanic waveguide in the several months following

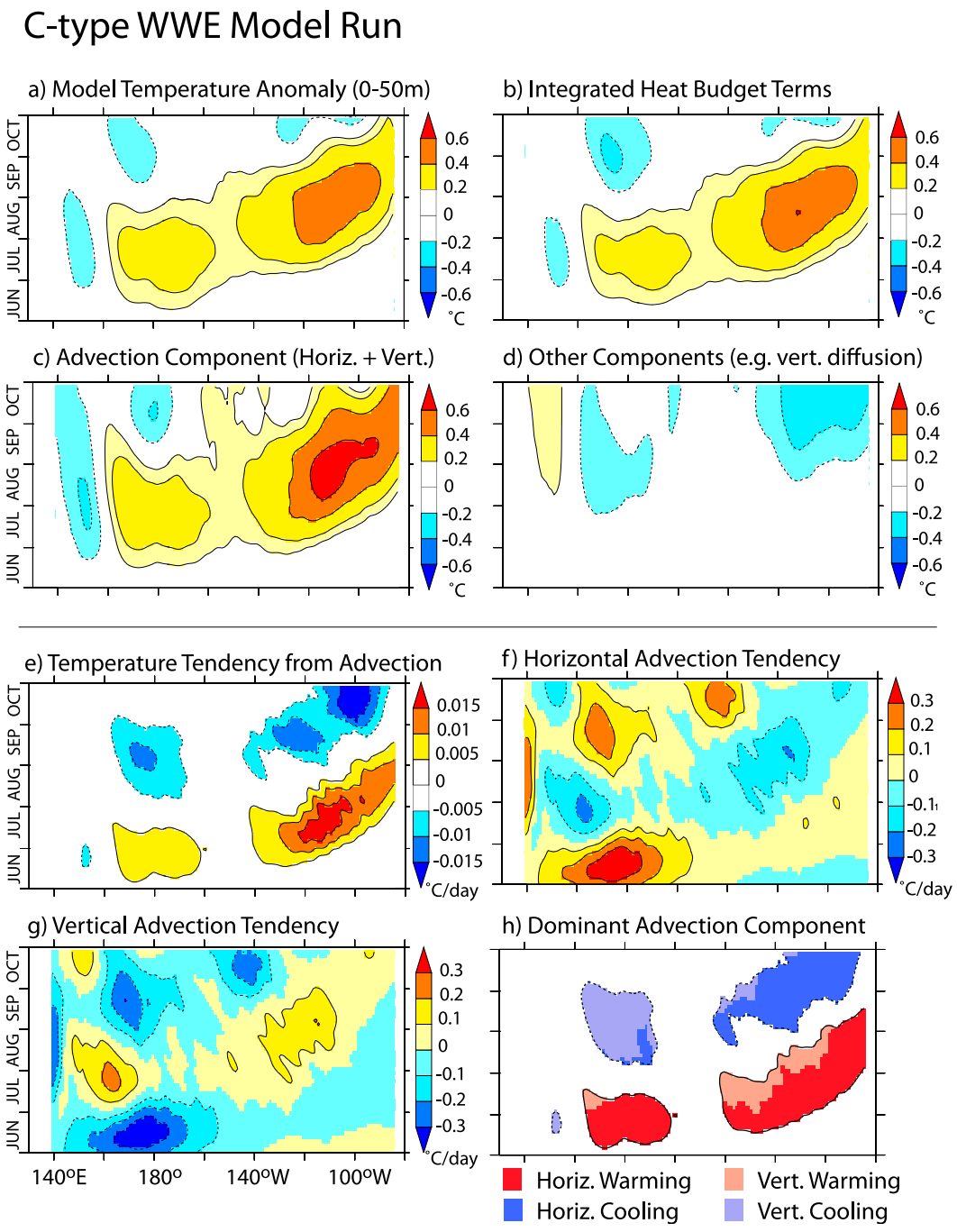

FIG. 8. Near-surface ocean heat budget diagnostics from a C-type WWE model experiment: (a) 0–50-m average heat content anomaly, (b) integration of all heat budget anomaly components, (c) advection component of the heat budget, (d) sum of other components such as vertical diffusion and surface heat flux, (e) temperature tendency due to advection, (f) horizontal advection component, and (g) vertical advection component. (h) The dominant component of the temperature tendency due to advection (shading), where tendency magnitude exceeds 0.1°C day^{-1}.

their occurrence. We have examined the model behavior following the application of each type of WWE discussed here (W, C, and E) and found qualitatively similar results in this case. Thus, we have chosen to present just one set of results here (the C type) rather than unnecessarily lengthen the manuscript.

Figure 8a shows, again in the time–longitude perspective, the equatorial upper ocean (0–50 m and 2°S–2°N

average) temperature anomaly that is produced in the model following the application of a C-type WWE wind anomaly. Figure 8b shows the result of integrating the sum of each of the terms in the model heat budget (horizontal and vertical advection of the temperature gradient, surface heat flux, diffusion, etc.). The close correspondence between the temperature anomaly patterns shown in Figs. 8a and 8b confirms that the terms we examine accurately represent the warming actually seen in the model. In Figs. 8c and 8d, the anomaly seen in Fig. 8b is separated into two components; that driven by changes in ocean circulation (Fig. 8c) and that produced by other processes (e.g., vertical diffusion and surface heat flux) that we have chosen to sum after finding that the anomaly seen in Fig. 8a is driven predominantly by the circulation changes. In Figs. 8e–h we further examine these circulation anomaly effects. The temperature tendency that produces the anomaly seen in Fig. 8c (i.e., the first derivative of the advection-driven temperature anomaly) is shown in Fig. 8e. In Figs. 8f and 8g this temperature tendency is split into parts driven by horizontal and vertical changes in circulation, respectively. This reveals that the horizontal and vertical advection terms (specifically the horizontal and vertical heat flux divergence anomalies) are each much larger in amplitude than the net temperature tendency seen in the model, but have very similar oppositely signed patterns. Thus, the warming seen in the model results from there being a small imbalance between these two much larger, nearly compensating terms. To more clearly gauge which component drives or damps the net change in temperature, in Fig. 8h we have shaded the time and space where there is $>0.015°C\,day^{-1}$ net warming. The shading hue and value are chosen as follows: red if warming is greater than cooling, blue otherwise and dark if horizontal is greather than vertical, light otherwise. We thereby see that the initial (June–July) near–date line warming occurs because the horizontal (warming) component dominates the vertical (cooling) component then. The resulting warm SSTA in this location then subsides mainly because of the effects of vertical (cooling) advection. Farther east, the larger-amplitude warming that occurs in the cold tongue can also be seen to be mainly dominated by the effects of horizontal (warming) advection, although the vertical and horizontal components do switch roles in the later warming stages in the latitudes between 140° and 110°W. This eastern Pacific patch of warm SSTA later diminishes in amplitude resulting from the effects of horizontal (cooling) circulation changes. Examining the model current anomalies, we have confirmed that the horizontal advection anomalies discussed above are driven mainly by changes in the zonal rather than meridional component (not shown for brevity).

The same type of diagnostic analysis has been performed on a model experiment in which a composite MJO wind stress anomaly, based just on MJO events that contain a C-type WWE, was used to drive the model. In this case, an initial June–July cooling is seen in the eastern Pacific (~140°–80°W) attributable to the presence of the MJO-related surface easterlies in the applied wind composite. Following this initial cooling, however, the diagnostic results (Fig. 9) reveal that the ocean processes that create warm upper ocean temperatures following this MJO with C-type WWE wind anomaly are similar in character to those that cause the warming in the C-type WWE case discussed above. Here again, the cold tongue warming that is seen 2–3 months after the application of the wind anomaly is mainly driven by anomalous horizontal temperature advection. It may be noted, however, that in this case the vertical advection component also contributes to some of the later warming seen in the 140°–110°W longitude band (with horizontal advection in this case reversing from its otherwise warming tendency).

Cold tongue warming like that seen following a WWE or MJO with WWE is not seen following the application of the composite MJO wind anomaly that is based on just the events that do not contain an embedded WWE (Fig. 10). As in the two experiments discussed above, however, the temperature changes that are seen in this case are still initiated and mainly driven by wind-driven changes in horizontal advection.

In summary, it is mainly the wind-driven changes in the horizontal (zonal) ocean heat flux divergence that are responsible for the equatorial warming that is seen in the model following the application of WWE-related wind anomalies. It should be recognized, however, that the equatorial warming that occurs in the model results from a small imbalance between two large (horizontal heating + vertical cooling) components.

8. Distribution of MJO events and WWEs

In this section we more closely examine the relationship between the timing of the MJO and WWEs, focusing mainly but not exclusively on the events occurring in ENSO-neutral conditions. Our intent is to determine whether the presence of the MJO affects the likelihood that a WWE will occur. To do this we determine the numbers of MJO events that do and do not contain a WWE, as well as the numbers of WWEs that occur and do not occur during an MJO event. The historical distributions of events will be compared to those produced in a Monte Carlo simulation that randomly distributes the same number of events throughout the period(s) considered to identify any characteristics of the

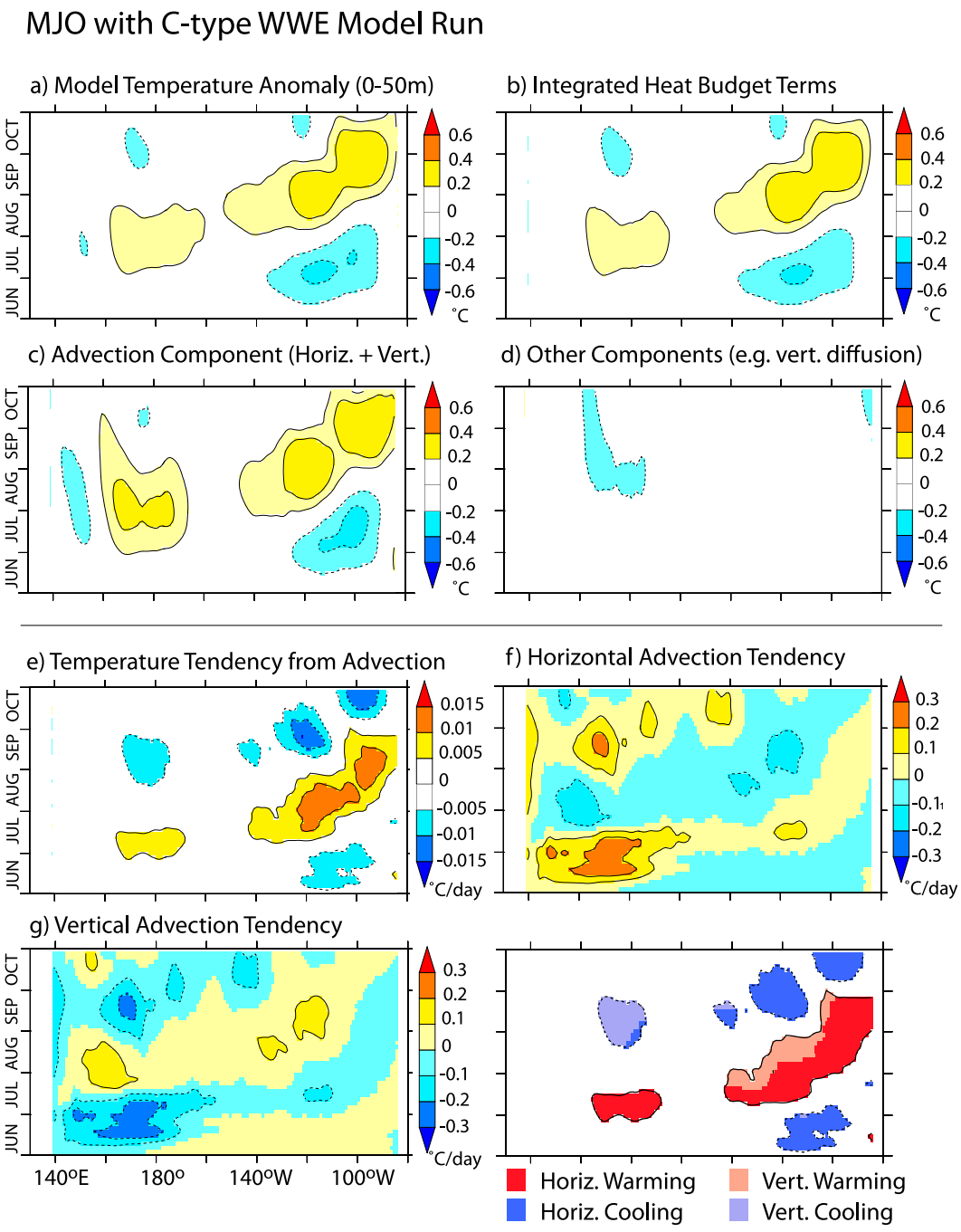

FIG. 9. As in Fig. 8, but for the MJO with WWE model experiment.

observed distributions that cannot be easily explained by the effects of random selection alone.

The respective categories of MJO and WWEs are defined as follows. An MJO event that contains a WWE is one in which the start day of at least one W-, C-, or E-type WWE occurs during it. The remaining MJO events do not contain a WWE. As described in the methods section, WWEs are defined as days in which the defining-region average wind speed anomaly is $>2\,\mathrm{m\,s^{-1}}$ for at least 3 consecutive days, with the WWE start day being the first of these days. A WWE that occurs during an MJO event is one in which the start day occurs during one of the identified MJO events. The remaining WWEs do not occur during an MJO event.

For each ENSO condition considered, there are some MJO events that do and some that do not contain a WWE,

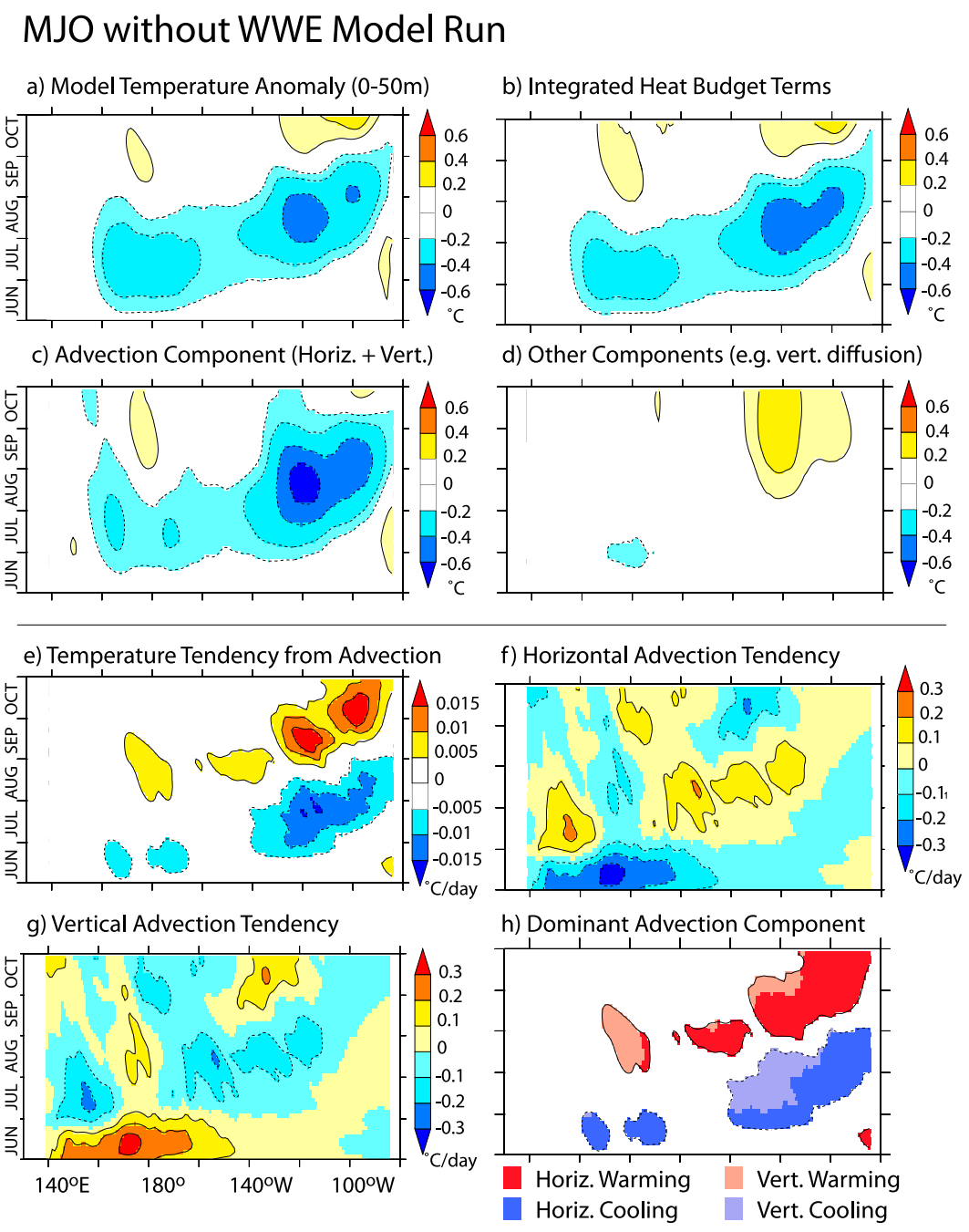

FIG. 10. As in Fig. 8, but for the MJO without WWE model experiment.

but not in equal numbers (Table 2). Over all ENSO conditions, the number of MJO events with a WWE exceeds the number that do not contain a WWE, but what does this result say about whether or not the chance of seeing a WWE is affected by the state of the MJO? To decide this properly, the characteristic duration and frequency of the MJO, as well as frequency of WWEs, must be taken into account.

In ENSO-neutral conditions there were 64 MJO events identified, including 43 that contain a WWE and 21 that do not. Based on the definitions used here, the MJO was in "event state" 40% of the time that the Niño-3 index had magnitude <0.75°C in the 1986–2010 period. During this same time there were 256 WWEs identified with start days in ENSO-neutral conditions. We performed bootstrap Monte Carlo simulations

TABLE 2. Distribution of MJO events by ENSO state and WWE activity.

	No. of MJO events		
	Total	With WWE	No WWE
All-time	112	75	37
ENSO-neutral	64	43	21
Warm-ENSO	26	25	1

(N = 10 000) to test whether the observed fraction of MJO events with or without a WWE is unusual compared to those expected based on a purely random scattering of this number of WWEs about the identified time history of MJO activity. The average values and the 5% and 95% confidence levels from the Monte Carlo simulations are shown in Fig. 11, where it can be seen that the observed number of MJO events that contain a WWE (43) is very close to the most likely value (44; to the nearest whole number), and well within the 5% (39) and 95% (50) confidence levels. It follows that the observed number of MJO events that do not contain a WWE also fits easily within the simulated (random) distribution. Thus, the null hypothesis, that WWE likelihood remains the same whether or not an MJO event occurs, holds for ENSO-neutral conditions. Trial has shown that this remains true even when the subset of 61 MJO events that reach their surface-Pacific-westerly phase in ENSO-neutral conditions (as discussed in section 3) is considered.

It is evident from the values in Table 2 that the fraction of MJO events with a WWE greatly increases moving from ENSO-neutral to warm-ENSO conditions, during which time 25 out of 26 MJO were observed to

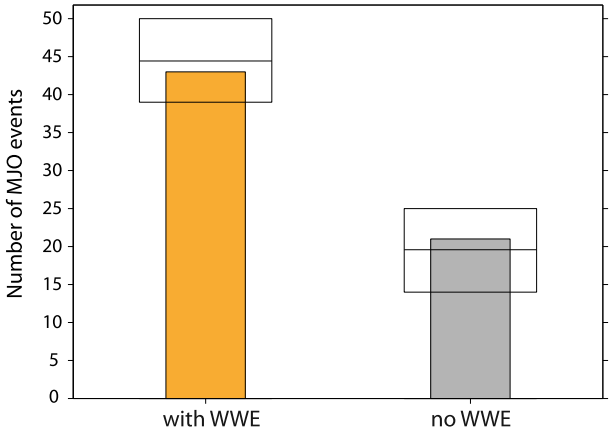

FIG. 11. Number of MJO events that do and do not contain a WWE for the period 1986–2010 and |Niño-3| < 0.75°C. The top, middle, and bottom horizontal lines about each bar show the p = 0.95, expected, and p = 0.05 levels, respectively, based on a random distribution of events.

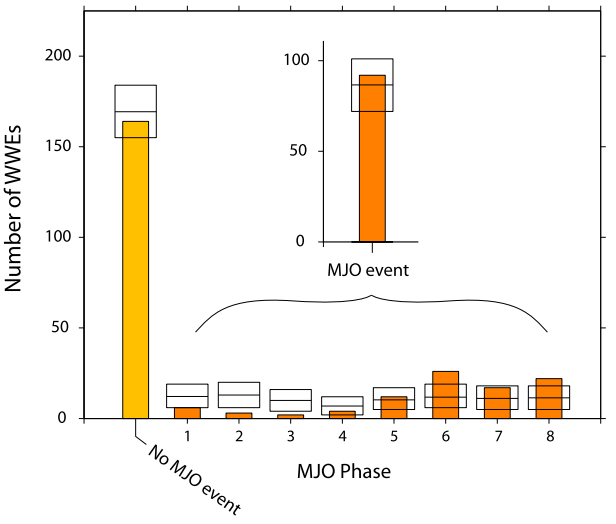

FIG. 12. The numbers of WWEs that do and do not occur during an MJO event, listed by MJO phase (based on WWE start date) for the co-occurring case. Horizontal lines are the p = 0.95, expected, and p = 0.05 values as in Fig. 11.

contain a WWE. It came initially as some surprise to the authors to find that results from the same type of Monte Carlo simulation as described above, except applied to the warm-ENSO (Niño-3 > 0.75°C) portion of the record, show that even this result is not statistically significant—that is, not much different than should be expected based on random selection of WWE start times. This can be understood by considering that although the fractions of time that the MJO is in event state in both ENSO-neutral and ENSO-warm conditions

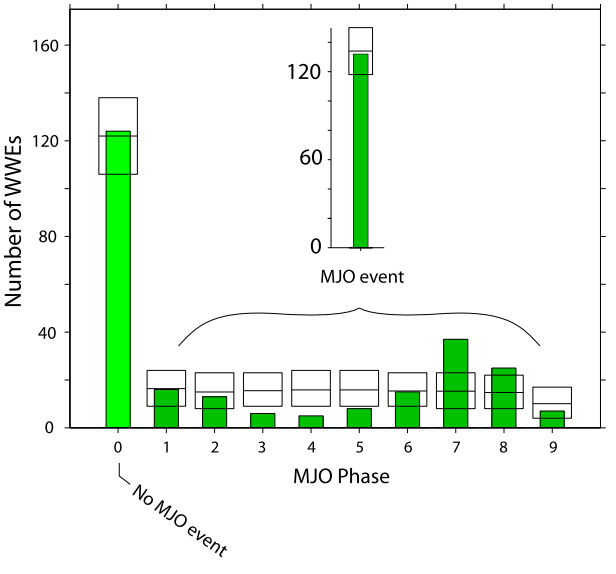

FIG. 13. As in Fig. 12, but using the MH98 index for MJO event identification.

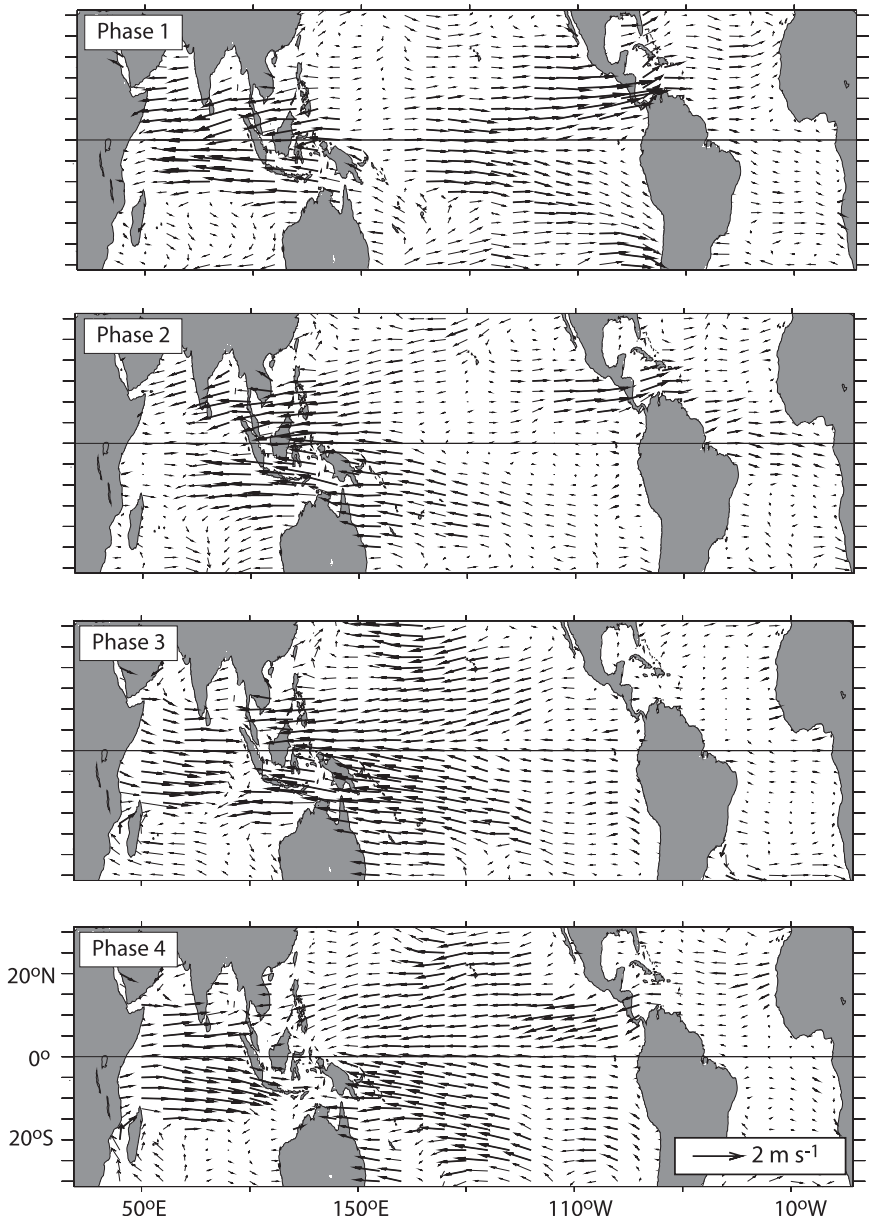

FIG. A1. Composite MJO wind anomalies. Thick arrows highlight anomalies that reach the 95% confidence level based on Monte Carlo bootstrap methods.

are about the same, the frequency of WWEs increases substantially moving from neutral to warm-ENSO conditions. Specifically, the WWE frequency increases from approximately 1.3 month^{-1} (256 WWEs in 5784 days) in ENSO-neutral to approximately 2.4 month^{-1} (136 WWEs in 1744 days) in warm-ENSO conditions. This increase in WWE frequency as the ENSO SSTAs warm is consistent with the findings of Harrison and Vecchi (1997) and Vecchi and Harrison (2000), which were based on a substantially shorter record, along with the many other aforementioned studies (e.g., Lengaigne et al. 2004; Vecchi et al. 2006; Eisenman et al. 2005; Gebbie et al. 2007; Gebbie and Tziperman 2009a,b) that have examined the dependence of WWE frequency on ENSO state. Because of the relatively high frequency of WWEs in warm-ENSO conditions, it simply becomes rather difficult to randomly choose an MJO-event-sized time span that does not contain at least 1 WWE in warm ENSO conditions. The most common Monte Carlo result in this case was finding that 23 of the 26 MJO events contained at least one randomly scattered WWE. Although the observed number (25) is slightly larger, it is

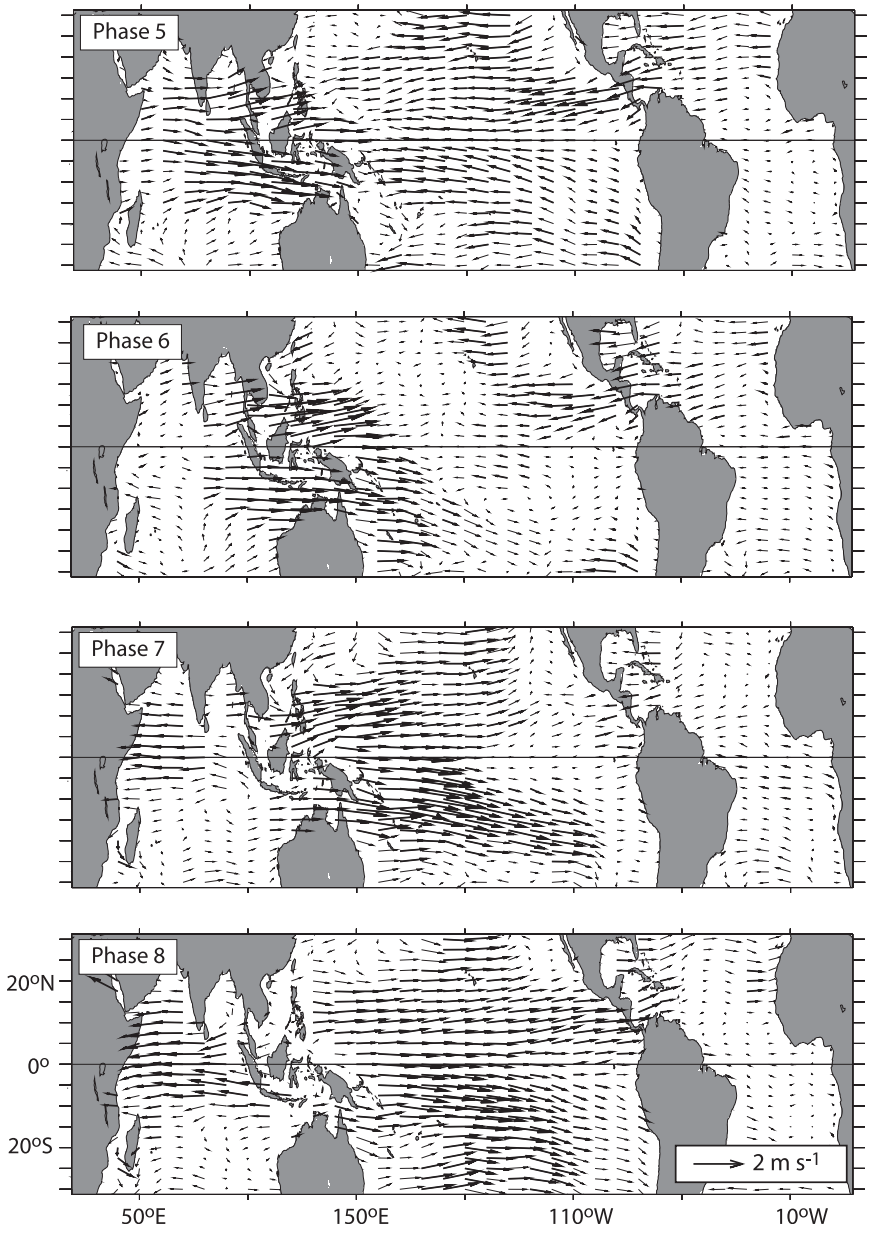

FIG. A1. (*Continued*)

not statistically significant at standard ($p > 0.8$) confidence levels.

As a point of comparison, it is notable that results comparable to Seiki and Takayabu's (2007) finding, based on different MJO and WWE definitions than used here, that the fraction of MJO events that contain WWEs tends to increase with MJO amplitude (cf. their Fig. 14) can also be seen in the distribution of events discussed here. When the 64 ENSO-neutral MJO events we identify are ranked based on the maximum daily MJO amplitude attained during the event, for example, it is revealed that 9 of the top 10 and all 5 of the top-5-ranked MJO events contain WWEs. Before imputing meaning to this result, however, it is important to test the null hypothesis that such a result can easily be explained by chance. In this case, Monte Carlo results again show that it can. It bears noting that another characteristic of MJOs that increases with amplitude is their length; there is almost a factor of 2 difference between the average lengths of all 64 MJO events (32 days) and the top-ranked events (51 and 56 days in the top-10 and top-5 cases, respectively). It is simply difficult to randomly choose such (longer than

average) lengths of time without bracketing at least one of the 256 WWEs observed in the period considered. In each case (top 5 and top 10), there was a better than 50% chance that the number of MJO-with-WWE events found by the Monte Carlo model met or exceeded the numbers (9 of 10, and 5 of 5) seen in the observed record. Thus, this is not a statistically significant relationship. Our results therefore do not support the Seiki and Takayabu (2007) hypothesis that large-amplitude MJO events are especially conducive to WWEs.

We have also used Monte Carlo methods to examine the corresponding question of whether the distribution of WWEs with respect to MJO state shows any significant deviations from that expected based on chance alone. The results we find in this case are consistent with those discussed above in that both the total number of WWEs that do (92) and do not (164) occur during the MJO events identified in ENSO-neutral conditions (Fig. 12; yellow bar and inset orange bar, respectively) are not significantly different from the values expected based on random chance alone.

Upon closer inspection, however, we do see that when they co-occur, WWEs tend to avoid the phases of the MJO with surface easterlies in the tropical Pacific (especially phases 1, 2, and 3) and instead frequent the later westerly phases (especially phases 6 and 8). Although it may be at first tempting to some to draw conclusions based just on this increase in WWE frequency in phases 6 and 8 (or decrease in earlier phases), it must also be recognized that the commensurate decrease in WWE frequency during the surface easterly MJO phases means that the overall likelihood of seeing a WWE is not significantly changed by the presence of the MJO, unless the MJO is somehow able to start and end in its surface westerly phase over the western equatorial Pacific without passing through its surface easterly phases, which is not its characteristic behavior.

In summary, we find that when they do co-occur, there is a tendency for the WWEs to frequent the surface westerly phases of the MJO and avoid, in nearly equal numbers, the surface easterly phases of the MJO such that that the overall likelihood of seeing a WWE is not changed by the presence of the MJO, even in extreme MJO-amplitude cases. This finding is confirmed when MJO events are identified using the Maloney and Hartmann (1998) MJO definition (Fig. 13).

9. Summary and discussion

Our composites of SSTA changes observed over the last 25 years show that anomalous waveguide warming, upward of a few tenths of a degree Celsius, is seen, in an average sense, following the W-, C-, and E-type WWEs that occurred during ENSO-neutral conditions. Over this time, warming anomalies with similar amplitudes and patterns are seen in the composites regardless of whether they include just WWEs that do or do not occur during an MJO event. This same type of warming anomaly is seen, in an average sense, following the contemporaneous MJO events that contain embedded WWEs, but is not seen following the MJO events that do not have embedded WWEs.

Integration of composite WWE and MJO wind stress anomalies in a realistic primitive equation model of the upper tropical Pacific is able to reproduce these results, in the sense that composite WWE wind stresses, and (to a lesser extent) wind stress composites from MJOs that contain WWEs, drive comparable warm-SSTA anomalies in the model. However, this type of warming is not seen in the model following composite MJO events that do not contain embedded WWEs.

These results confirm that WWE wind stress anomalies are important to the onset of El Niño events. Because waveguide warming is not seen following an MJO unless it contains a WWE and the chances of seeing a WWE remain the same whether or not an MJO event occurs, the same cannot be said for the MJO, however. This confirms the findings of Vecchi (2000), with a near doubling of period, while on the other hand contradicting some previous hypotheses that the MJO itself plays an important role in initiating El Niño events. Although direct comparison between previous studies of MJO effects on SSTA and ours is made difficult by the fact that different MJO definitions have generally been used in each case (cf. Kessler and Kleeman 2000; Zhang and Gottschalck 2002; Hendon et al. 2007; Seiki and Takayabu 2007; Seiki et al. 2009; Kapur et al. 2012), we suggest that the results of this study, which dissects the interrelationships between each class of wind event and the changes in waveguide SSTA that follow them, nonetheless provide a generally useful perspective from which to better understand the seemingly disparate claims about WWE and MJO effects that exist in the published literature.

The co-occurrence of MJO and westerly wind events, as defined here, is common enough that it is not difficult to find MJO events with embedded WWEs regardless of the definitions used, and it is evident that waveguide warming, like that which follows solo WWEs, will often be seen following the MJO events that contain a WWE. Further, it is reasonable to expect that different MJO definitions will capture relatively more or less of the effects of these WWEs, but the results discussed here strongly suggest that even the most skillful prediction of the state of the MJO will not be useful in predicting the development of El Niño events since the MJO does not itself contribute to waveguide warming, nor does it affect the overall likelihood, even in the case of extreme-amplitude MJO events, of seeing a WWE.

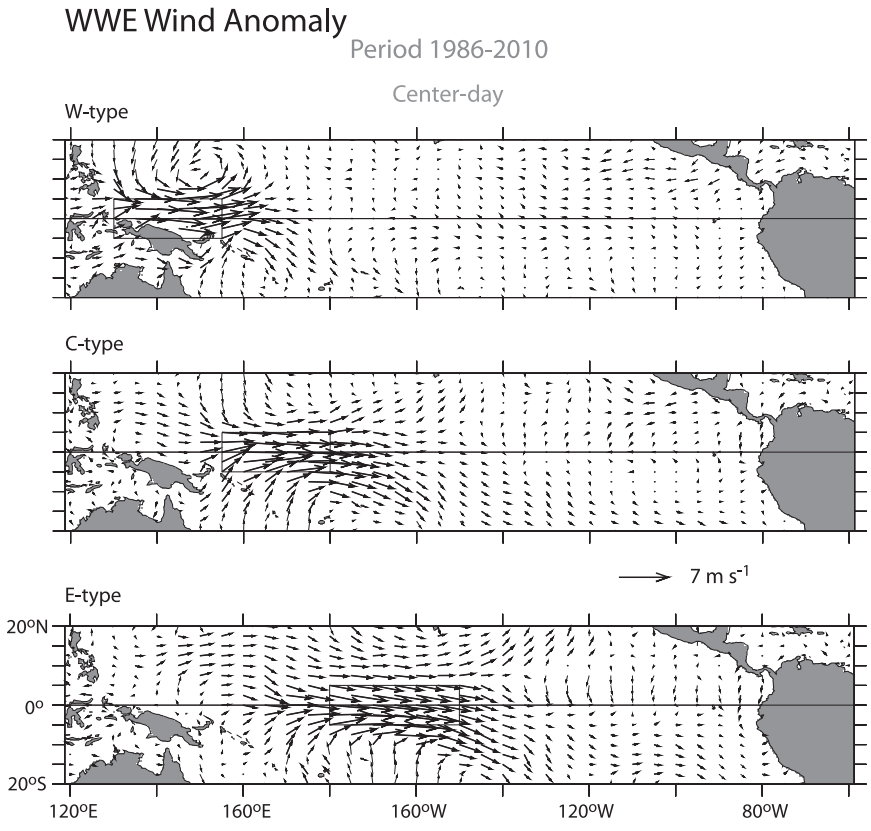

FIG. A2. Westerly wind event wind anomalies. Thick arrows highlight anomalies that reach the 95% confidence level based on Monte Carlo bootstrap methods.

On the other hand, our results are consistent with (although do not explain) previous findings that WWE frequency increases with the transition from ENSO-neutral to warm-ENSO conditions, thereby increasing the influence of WWEs on ENSO (Harrison and Vecchi 1997; Vecchi and Harrison 2000; Lengaigne et al. 2004; Eisenman et al. 2005; Vecchi et al. 2006; Gebbie et al. 2007; Gebbie and Tziperman 2009a,b; Harrison and Chiodi, 2009). That is, although WWEs are high frequency and the details of each event have a substantial stochastic component, the strong relationship between WWE frequency and ENSO state makes WWEs, to a large degree, an element of the slow coupled ocean–atmosphere processes that help drive and maintain equatorial Pacific waveguide warming during El Niño events. WWEs are not best thought of as external ''additive'' noise.

Thus, forming a better understanding of the sources and predictability of WWEs remains an avenue for improving our understanding of the mechanisms for initiation and potential predictability of an El Niño event, but it does not seem that effort to better understand the MJO, although potentially quite useful in many other important respects, will provide this.

Acknowledgments. This publication is (partially) funded by the Joint Institute for the Study of the Atmosphere and Ocean (JISAO) under NOAA Cooperative Agreement NA10OAR4320148, Contribution 2021, and by support from the Climate Observations Division of the NOAA Climate Program Office as well as from NOAA's Pacific Marine Environmental Laboratory (PMEL). We thank M. Lengaigne for helpful comments and the anonymous reviewers.

APPENDIX A

MJO and WWE Composite Wind Anomalies

Figure A1 shows the composite wind anomalies for each phase of the MJO. In this case the composites are averages of the daily wind anomalies for each day that the MJO amplitude was >1 and the MJO was in the given phase. Only ENSO-neutral days are considered in this case.

Figure A2 shows the day-0 composite wind anomalies for the W-, C-, and E-type WWEs that occurred in ENSO-neutral conditions in the 1986–2010 period. In each case, the anomalies with statistically significant zonal components are marked by thickened vectors.

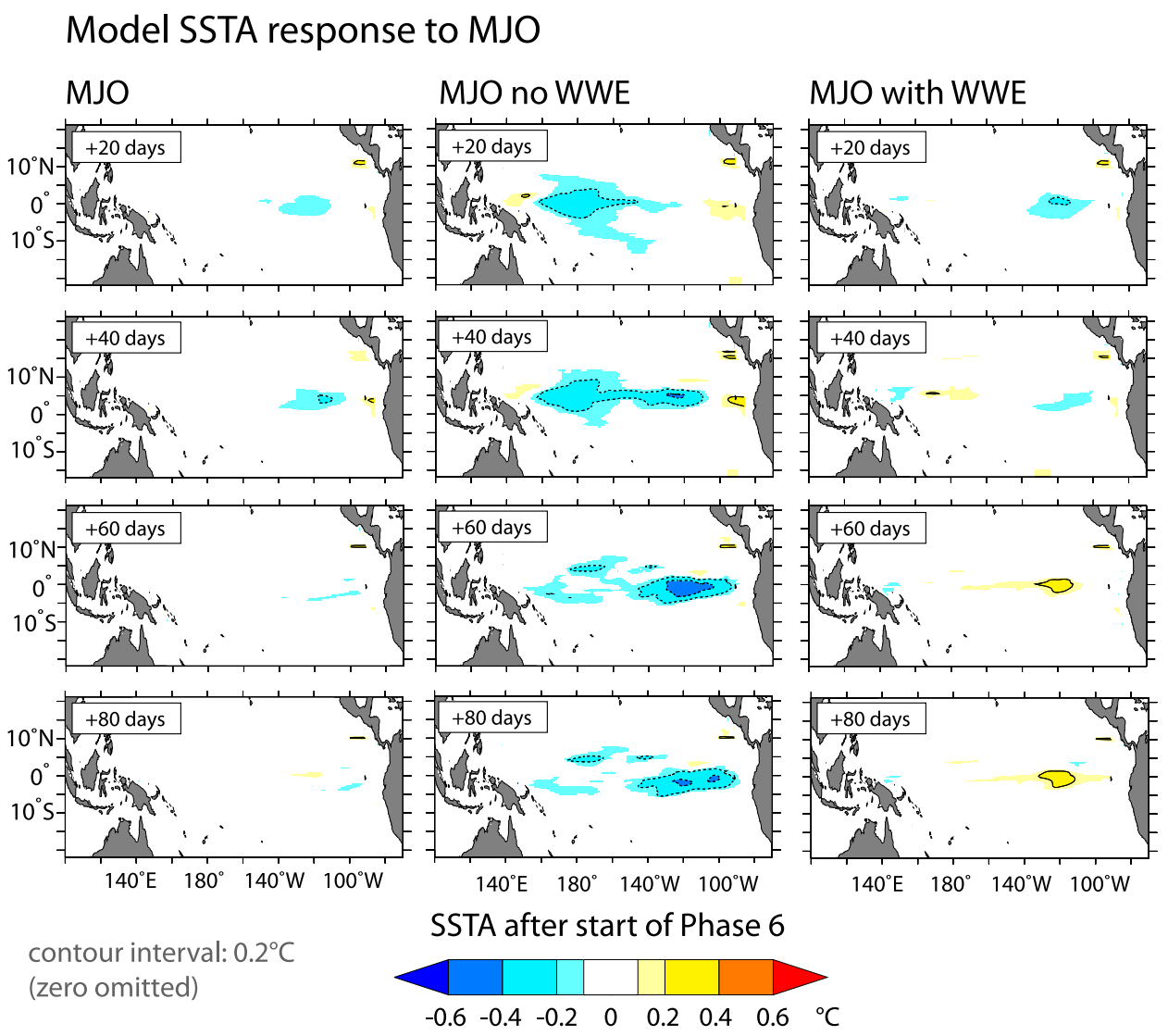

FIG. C1. Model SSTA following the application of a (variable phase duration) composite MJO wind stress anomaly.

APPENDIX B

Monte Carlo Methods

This appendix describes the methods used for determining whether or not the anomaly magnitudes seen in the composites of observed variables (e.g., SSTA changes following the MJO and WWEs and event composite wind anomalies) can easily be obtained by random selection of dates, or instead, whether they are statistically significant. This process is conceptually straightforward in that the compositing procedure used for the observations is simply repeated in the Monte Carlo simulation, except that in the Monte Carlo case the composited days are chosen randomly. Specifically, a number of days are randomly chosen from the distribution of days considered (e.g., all those in which |Niño-3| < 0.75°C) and averaged, repeatedly, to build up a distribution of possible outcomes, to which the observed result is compared. If the observed result lies at the narrow tail of this distribution (e.g., $p > 0.95$) then it is considered statistically significant. If the likelihood of getting the observed result by chance is higher than this, they are not.

In such statistical methods it is often important that the number of effectively independent samples contained in the actual and bootstrap composites be consistent with one another. Traditionally, the number of degrees of freedom in the actual composite has been determined as a function of the sample autocorrelation function (ACF) (e.g., Leith 1973). Here, we use a procedure that yields results consistent with the traditional

methods but avoids the burden of calculating the ACF at each grid point considered. Instead, we rely on the observed frequency of events to reproduce the effects of any observations that may lie within an effective time between independent samples. To do this we begin at a random date within the subset of dates considered, and then select samples from the (modulo) historical record, with sample-to-sample time lags randomly chosen from the observed time lags that lie within the continuous ENSO-neutral periods, until the bootstrap and observed SSTA-change composites contain the same number of samples. In this way, the average effects of closely spaced observations (i.e., observations that occur too close together in time to be considered independent of one another) is reproduced in the bootstrap procedure in a manner consistent with the observations. We chose this method since it alleviates the computationally intensive need to determine autocorrelation characteristics for each of the (spatially varying) fields considered. Trial has shown that the difference between including and not including these effects of closely spaced observations on the estimated confidence intervals, though not negligible, can be neglected without fundamentally changing the results discussed here (i.e., the timings of the WWEs and MJO events are such that each can almost be considered to be associated with an independent sample of the target variable).

APPENDIX C

Model Response to Composite MJO Wind Anomalies (with Variable Phase Duration)

Figure C1 shows the results of applying an idealized MJO composite wind stress anomaly to the ocean model. The results in this figure were obtained by the same experimental procedure used to produce the results shown in Fig. 5, except in this case the specified MJO-phase duration varies according to the average duration observed in the identified MJO events, which ranges from 3 to 5.5 days and is 4.5 days on average.

REFERENCES

Belamari, S., J. L. Redelsperger, and M. Pontaud, 2003: Dynamic role of a westerly wind burst in triggering an equatorial Pacific warm event. *J. Climate,* **16,** 1869–1890, doi:10.1175/1520-0442(2003)016<1869:DROAWW>2.0.CO;2.

Chen, S. S., R. A. Houze, and B. E. Mapes, 1996: Multiscale variability of deep convection in relation to large-scale circulation in TOGA COARE. *J. Atmos. Sci.,* **53,** 1380–1409, doi:10.1175/1520-0469(1996)053<1380:MVODCI>2.0.CO;2.

Eisenman, I., L. Yu, and E. Tziperman, 2005: Westerly wind bursts: ENSO's tail rather than the dog? *J. Climate,* **18,** 5224–5238, doi:10.1175/JCLI3588.1.

Gebbie, G., and E. Tziperman, 2009a: Predictability of SST-modulated westerly wind bursts. *J. Climate,* **22,** 3894–3909, doi:10.1175/2009JCLI2516.1.

——, and ——, 2009b: Incorporating a semi-stochastic model of ocean-modulated westerly wind bursts into an ENSO prediction model. *Theor. Appl. Climatol.,* **97,** 65–73, doi:10.1007/s00704-008-0069-6.

——, I. Eisenman, A. Wittenberg, and E. Tziperman, 2007: Modulation of westerly wind bursts by sea surface temperature: A semistochastic feedback for ENSO. *J. Atmos. Sci.,* **64,** 3281–3295, doi:10.1175/JAS4029.1.

Giese, B. S., and D. E. Harrison, 1990: Aspects of the Kelvin wave response to episodic wind forcing. *J. Geophys. Res.,* **95,** 7289–7312, doi:10.1029/JC095iC05p07289.

——, and ——, 1991: Eastern equatorial Pacific response to three composite westerly wind types. *J. Geophys. Res.,* **96,** 3239–3248, doi:10.1029/90JC01861.

Gill, A. E., 1980: Some simple solutions for heat-induced tropical circulation. *Quart. J. Roy. Meteor. Soc.,* **106,** 447–462, doi:10.1002/qj.49710644905.

Gnanadesikan, A., and Coauthors, 2006: GFDL's CM2 global coupled climate models. Part II: The baseline ocean simulation. *J. Climate,* **19,** 675–697, doi:10.1175/JCLI3630.1.

Griffies, S. M., M. J. Harrison, R. C. Pacanowski, and A. Rosati, 2003: A technical guide to MOM 4. GFDL Ocean Group Tech. Rep. 5, 295 pp.

Harrison, D. E., 1984: The appearance of sustained equatorial surface westerlies during the 1982 Pacific warm event. *Science,* **224,** 1099–1102, doi:10.1126/science.224.4653.1099.

——, and P. S. Schopf, 1984: Kelvin-wave-induced anomalous advection and the onset of surface warming in El Niño events. *Mon. Wea. Rev.,* **112,** 923–933, doi:10.1175/1520-0493(1984)112<0923:KWIAAA>2.0.CO;2.

——, and B. S. Giese, 1991: Episodes of surface westerly winds as observed from islands in the western tropical Pacific. *J. Geophys. Res.,* **96** (Suppl.), 3221–3237, doi:10.1029/90JC01775.

——, and G. A. Vecchi, 1997: Westerly wind events in the tropical Pacific, 1986–95. *J. Climate,* **10,** 3131–3156, doi:10.1175/1520-0442(1997)010<3131:WWEITT>2.0.CO;2.

——, and A. M. Chiodi, 2009: Pre- and post-1997/98 westerly wind events and equatorial Pacific cold tongue warming. *J. Climate,* **22,** 568–581, doi:10.1175/2008JCLI2270.1.

——, ——, and G. A. Vecchi, 2009: Effects of surface forcing on the seasonal cycle of the eastern equatorial Pacific. *J. Mar. Res.,* **67,** 701–729, doi:10.1357/002224009792006179.

Hartten, L. M., 1996: Synoptic settings of westerly wind bursts. *J. Geophys. Res.,* **101,** 16 997–17 019, doi:10.1029/96JD00030.

Hendon, H. H., M. C. Wheeler, and C. Zhang, 2007: Seasonal dependence of the MJO–ENSO relationship. *J. Climate,* **20,** 531–543, doi:10.1175/JCLI4003.1.

Kapur, A., C. Zhang, J. Zavala-Garay, and H. Hendon, 2012: Role of stochastic forcing in ENSO in observations and a coupled GCM. *Climate Dyn.,* **38,** 87–107, doi:10.1007/s00382-011-1070-9.

Keen, R. A., 1982: The role of cross-equatorial cyclone pairs in the Southern Oscillation. *Mon. Wea. Rev.,* **110,** 1405–1416, doi:10.1175/1520-0493(1982)110<1405:TROCET>2.0.CO;2.

Kessler, W. S., 2001: EOF representations of the Madden–Julian oscillation and its connection with ENSO. *J. Climate,* **14,** 3055–3061, doi:10.1175/1520-0442(2001)014<3055:EROTMJ>2.0.CO;2.

——, and M. J. McPhaden, 1995: Oceanic equatorial waves and the 1991–93 El Niño. *J. Climate,* **8,** 1757–1774, doi:10.1175/1520-0442(1995)008<1757:OEWATE>2.0.CO;2.

——, and R. Kleeman, 2000: Rectification of the Madden–Julian oscillation into the ENSO cycle. *J. Climate,* **13,** 3560–3575, doi:10.1175/1520-0442(2000)013<3560:ROTMJO>2.0.CO;2.

Kindle, J. C., and P. A. Phoebus, 1995: The ocean response to operational westerly wind bursts during the 1991–1992 El Niño. *J. Geophys. Res.,* **100,** 4893–4920, doi:10.1029/94JC02392.

Larkin, N. K., and D. E. Harrison, 2002: ENSO warm (El Niño) and cold (La Niña) event life cycles: Ocean surface anomaly patterns, their symmetries, asymmetries, and implications. *J. Climate,* **15,** 1118–1140, doi:10.1175/1520-0442(2002)015<1118:EWENOA>2.0.CO;2.

Leith, C. E., 1973: The standard error of time-average estimates of climatic means. *J. Appl. Meteor.,* **12,** 1066–1069, doi:10.1175/1520-0450(1973)012<1066:TSEOTA>2.0.CO;2.

Lengaigne, M., J.-P. Boulanger, C. Menkes, S. Masson, G. Madec, and P. Delecluse, 2002: Ocean response to the March 1997 westerly wind event. *J. Geophys. Res.,* **107,** 8015, doi:10.1029/2001JC000841.

——, ——, ——, G. Madec, P. Delecluse, E. Guilyardi, and J. M. Slingo, 2003: The March 1997 westerly wind event and the onset of the 1997/98 El Niño: Understanding the role of the atmospheric response. *J. Climate,* **16,** 3330–3343, doi:10.1175/1520-0442(2003)016<3330:TMWWEA>2.0.CO;2.

——, E. Guilyardi, J. P. Boulanger, C. Menkes, P. Delecluse, P. Inness, J. Cole, and J. Slingo, 2004: Triggering of El Niño by westerly wind events in a coupled general circulation model. *Climate Dyn.,* **23,** 601–620, doi:10.1007/s00382-004-0457-2.

Lin, X., and R. H. Johnson, 1996: Kinematic and thermodynamic characteristics of the flow over the western Pacific warm pool during TOGA COARE. *J. Atmos. Sci.,* **53,** 695–715, doi:10.1175/1520-0469(1996)053<0695:KATCOT>2.0.CO;2.

Love, G., 1985a: Cross-equatorial influence of winter hemisphere subtropical cold surges. *Mon. Wea. Rev.,* **113,** 1487–1498, doi:10.1175/1520-0493(1985)113<1487:CEIOWH>2.0.CO;2.

——, 1985b: Cross-equatorial interactions during tropical cyclogenesis. *Mon. Wea. Rev.,* **113,** 1499–1509, doi:10.1175/1520-0493(1985)113<1499:CEIDTC>2.0.CO;2.

Luther, D. S., D. E. Harrison, and R. A. Knox, 1983: Zonal winds in the central equatorial Pacific and El Niño. *Science,* **222,** 327–330, doi:10.1126/science.222.4621.327.

Madden, R. A., and P. R. Julian, 1972: Description of global-scale circulation cells in the tropics with a 40–50 day period. *J. Atmos. Sci.,* **29,** 1109–1123, doi:10.1175/1520-0469(1972)029<1109:DOGSCC>2.0.CO;2.

Maloney, E. D., and D. L. Hartmann, 1998: Frictional moisture convergence in a composite life cycle of the Madden-Julian oscillation. *J. Climate,* **11,** 2387–2403, doi:10.1175/1520-0442(1998)011<2387:FMCIAC>2.0.CO;2.

McPhaden, M. J., 2004: Evolution of the 2002/03 El Niño. *Bull. Amer. Meteor. Soc.,* **85,** 677–695, doi:10.1175/BAMS-85-5-677.

Perigaud, C. M., and C. Cassou, 2000: Importance of oceanic decadal trends and westerly wind bursts for forecasting El Niño. *Geophys. Res. Lett.,* **27,** 389–392, doi:10.1029/1999GL010781.

Philander, S. G. H., and A. D. Seigel, 1985: Simulation of El Niño of 1982-1983. *Coupled Occean–Atmosphere Models,* J. Nihoul, Ed., Elsevier, 517–541.

Richardson, R. A., I. Ginis, and L. M. Rothstein, 1999: A numerical investigation of the local ocean response to westerly wind burst forcing in the western equatorial Pacific. *J. Phys. Oceanogr.,* **29,** 1334–1352, doi:10.1175/1520-0485(1999)029<1334:ANIOTL>2.0.CO;2.

Schopf, P. S., and D. E. Harrison, 1983: On equatorial waves and El Niño. I. Influence of initial states on wave-induced currents and warming. *J. Phys. Oceanogr.,* **13,** 936–948, doi:10.1175/1520-0485(1983)013<0936:OEWAEN>2.0.CO;2.

Seiki, A., and Y. N. Takayabu, 2007: Westerly wind bursts and their relationship with intraseasonal variations and ENSO. Part I: Statistics. *Mon. Wea. Rev.,* **135,** 3325–3345, doi:10.1175/MWR3477.1.

——, ——, K. Yoneyama, N. Sato, and M. Yoshizaki, 2009: The oceanic response to the Madden–Julian oscillation and ENSO. *SOLA,* **5,** 93–96, doi:10.2151/sola.2009-024.

Slingo, J. M., D. P. Rowell, K. R. Sperber, and F. Nortley, 1999: On the predictability of the interannual behavior of the Madden–Julian oscillation and its relationship with El Niño. *Quart. J. Roy. Meteor. Soc.,* **125,** 583–609, doi:10.1002/qj.49712555411.

Vecchi, G. A., 2000: Sub-seasonal wind variability and El Niño. Ph.D. thesis, University of Washington, 184 pp.

——, and D. E. Harrison, 2000: Tropical Pacific sea surface temperature anomalies, El Niño, and equatorial westerly wind events. *J. Climate,* **13,** 1814–1830, doi:10.1175/1520-0442(2000)013<1814:TPSSTA>2.0.CO;2.

——, A. T. Wittenberg, and A. Rosati, 2006: Reassessing the role of stochastic forcing in the 1997–1998 El Niño. *Geophys. Res. Lett.,* **33,** L01706, doi:10.1029/2005GL024738.

Wheeler, M. C., and H. H. Hendon, 2004: An all-season real-time multivariate MJO index: Development of an index for monitoring and prediction. *Mon. Wea. Rev.,* **132,** 1917–1932, doi:10.1175/1520-0493(2004)132<1917:AARMMI>2.0.CO;2.

Zavala-Garay, J., A. M. Moore, C. L. Perez, and R. Kleeman, 2003: The response of a coupled model of ENSO to observed estimates of stochastic forcing. *J. Climate,* **16,** 2827–2842, doi:10.1175/1520-0442(2003)016<2827:TROACM>2.0.CO;2.

——, C. Zhang, A. M. Moore, and R. Kleeman, 2005: The linear response of ENSO to the Madden–Julian oscillation. *J. Climate,* **18,** 2441–2459, doi:10.1175/JCLI3408.1.

——, ——, ——, A. T. Wittenberg, M. J. Harrison, A. Rosati, J. Vialard, and R. Kleeman, 2008: Sensitivity of hybrid ENSO models to unresolved atmospheric variability. *J. Climate,* **21,** 3704–3721, doi:10.1175/2007JCLI1188.1.

Zhang, C., and J. Gottschalck, 2002: SST anomalies of ENSO and the Madden–Julian oscillation in the equatorial Pacific. *J. Climate,* **15,** 2429–2445, doi:10.1175/1520-0442(2002)015<2429:SAOEAT>2.0.CO;2.